AD-A137 145 EFFECTS OF PREHEAT ON WELDMENTS OF NICOP STEEL(U) NAVAL 1/1
POSTGRADUATE SCHOOL MONTEREY CA R F BURNA SEP 83

UNCLASSIFIED F/G 11/6 NL

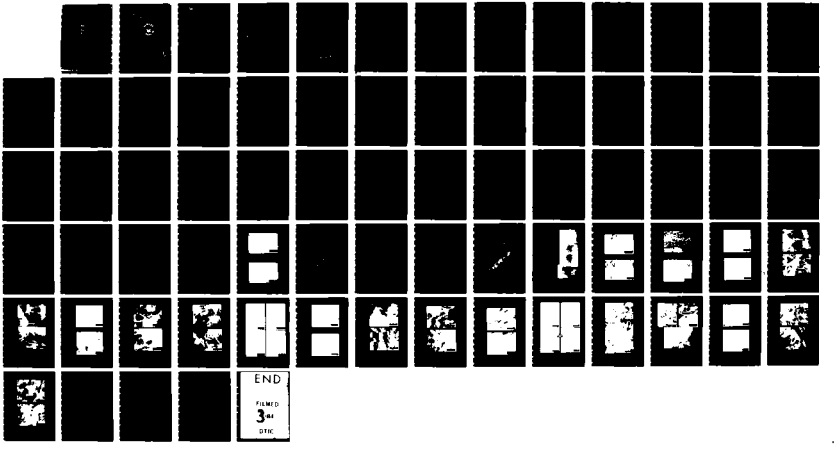

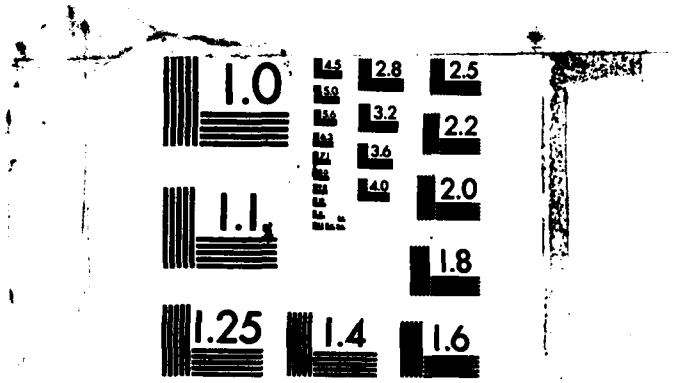

NAVAL POSTGRADUATE SCHOOL
Monterey, California

THESIS

EFFECTS OF PREHEAT ON WELDMENTS
OF NICOP STEEL

by

Richard F. Burna

September 1983

Thesis Advisor: K. D. Challenger

Approved for public release; distribution unlimited.

Unclassified

SECURITY CLASSIFICATION OF THIS PAGE (When Data Entered)

REPORT DOCUMENTATION PAGE	READ INSTRUCTIONS BEFORE COMPLETING FORM
1. REPORT NUMBER	2. GOVT ACCESSION NO. A137145 / 3. RECIPIENT'S CATALOG NUMBER
4. TITLE (and Subtitle) Effects of Preheat on Weldments of NICOP Steel	5. TYPE OF REPORT & PERIOD COVERED Master's Thesis; September 1983
	6. PERFORMING ORG. REPORT NUMBER
7. AUTHOR(s) Richard F. Burna	8. CONTRACT OR GRANT NUMBER(s)
9. PERFORMING ORGANIZATION NAME AND ADDRESS Naval Postgraduate School Monterey, California 93943	10. PROGRAM ELEMENT, PROJECT, TASK AREA & WORK UNIT NUMBERS
11. CONTROLLING OFFICE NAME AND ADDRESS Naval Postgraduate School Monterey, California 93943	12. REPORT DATE September 1983
	13. NUMBER OF PAGES 71
14. MONITORING AGENCY NAME & ADDRESS(if different from Controlling Office)	15. SECURITY CLASS. (of this report) Unclassified
	15a. DECLASSIFICATION/DOWNGRADING SCHEDULE

16. DISTRIBUTION STATEMENT (of this Report)

Approved for public release; distribution unlimited.

17. DISTRIBUTION STATEMENT (of the abstract entered in Block 20, if different from Report)

18. SUPPLEMENTARY NOTES

19. KEY WORDS (Continue on reverse side if necessary and identify by block number)

High Strength-Low Alloy (HSLA) Steels
NICOP
Preheat
Welding

20. ABSTRACT (Continue on reverse side if necessary and identify by block number)

Shielded metal arc weldments of Armco Steel Corporation's NICOP class 3, 19mm (3/4 inch) plate, conforming to ASTM A710 grade A, were studied to provide information concerning the microstructure in the heat affected zone (HAZ) of weldments fabricated with and without preheat. Microhardness, scanning electron microscopy and transmission electron microscopy were used to determine the effect of preheating on the microstructure.

DD FORM 1 JAN 73 1473 EDITION OF 1 NOV 65 IS OBSOLETE
S/N 0102-LF-014-6601

Unclassified
SECURITY CLASSIFICATION OF THIS PAGE (When Data Entered)

Similar microstructures in the preheat and non-preheat samples were observed. The microstructures were polygonal and acicular ferrite in the base and base/HAZ regions and increasing amounts of bainite and auto tempered martensite islands near the fusion line. From the point of view of microstructure, NICOP appears to be weldable without preheating.

Approved for public release; distribution unlimited.

Effects of Preheat on Weldments of NICOP Steel

by

Richard F. Burna
Lieutenant, United States Navy
B.S., University of Washington, 1977

Submitted in partial fulfillment of the
requirements for the degree of

MASTER OF SCIENCE IN MECHANICAL ENGINEERING

from the

NAVAL POSTGRADUATE SCHOOL
September 1983

Author: Richard F Burna

Approved by: Kenneth D Challenger
Thesis Advisor

Second Reader

P. J. Marto
Chairman, Department of Mechanical Engineering

J. M. Dyer
Dean of Science and Engineering

ABSTRACT

Shielded metal arc weldments of Armco Steel Corporation's NICOP class 3, 19mm (3/4 inch) plate, conforming to ASTM A710 grade A, were studied to provide information concerning the microstructure in the heat affected zone (HAZ) of weldments fabricated with and without preheat. Microhardness, scanning electron microscopy and transmission electron microscopy were used to determine the effect of preheating on the microstructure. Similar microstructures in the preheat and non-preheat samples were observed. The microstructures were polygonal and acicular ferrite in the base and base/HAZ regions and increasing amounts of bainite and auto tempered martensite islands near the fusion line. From the point of view of microstructure, NICOP appears to be weldable without preheating.

TABLE OF CONTENTS

LIST OF TABLES

LIST OF FIGURES

ACKNOWLEDGMENTS

I wish to express my appreciation to my thesis advisor, Dr. Ken Challenger, for his patience and guidance with this work. A special note of thanks to Dr. Parbir Deb for his invaluable assistance during the TEM and micrograph interpretation phases of this work. I would also like to thank Mr. Roger Fremier for his contribution of micrograph reproduction and photographic assistance throughout this effort. To my wife Bonnie and our children Candi, Jennifer and Richard, who have been a source of inspiration throughout my Naval career, I dedicate this work.

I. INTRODUCTION

A. DEVELOPMENT OF NICOP STEEL

During the last decade increased demand for steels with higher yield strengths, improved weldability and good toughness which could be economically produced encouraged the development of high strength-low alloy (HSLA) types of steel. These steels utilize microalloying element additions in small amounts and keep carbon levels below 0.15% to obtain the required strengths and toughness levels.

During the seventies a new low alloy steel was introduced which contains 1.0-1.3% copper with a maximum of 0.07% carbon. This steel is designated as ASTM A710 grade A for structural uses and can be furnished with three different heat treatments and strength levels. Class 1 designates as-rolled plates, class 2 normalized plates and class 3 plates are quenched. The final heat treatment for each class is precipitation hardening at 565 to 665^{o}C (1000 to 1225^{o}F) [Ref. 1]. Armco Steel Corporation produces this low alloy steel under the trade name NICOP.

B. INFLUENCE OF ALLOYING ELEMENTS ON NICOP STEEL

The primary strengthening mechanism is the 1.0-1.3% copper in this low alloy steel. Taken into solid solution in the austenite phase, the copper can precipitate as fine

epsilon-copper particles in ferrite. Air cooling from austenitizing temperatures causes considerable copper to remain in solid solution, however, quenching from elevated austenitizing temperatures results in even more copper in solid solution.

As ferrite transforms from austenite, or after ferrite has formed, some copper may precipitate as a fine epsilon copper phase in the ferrite as the solubility of copper is less in ferrite than in austenite. During cooling, equilibrium solubility is not reached and the subsequent heat treating to 565 to 665°C (1000 to 1225°F) permits additional epsilon copper phase to precipitate, allowing the desired properties to be obtained [Ref. 2].

Columbium is added for grain size refinement. If the columbium is allowed to dissolve in austenite the columbium will tend to retard ferrite formation and promote acicular or bainite structure formation. This effect is similar to that found in molybdenum alloyed steels. When molybdenum and columbium are combined in steels an intermediate transformation product, known as acicular ferrite, forms. Acicular ferrite differs from polygonal ferrite in it's size and dislocation density. The high density of fine columbium-molybdenum carbonitrides, high dislocation density and smaller grain size of acicular ferrite compared to steels with polygonal-ferrite give steels with acicular ferrite much higher strength [Ref. 3].

Nickel is added primarily to improve the steels toughness and strength. Nickel is also required in copper bearing steels to prevent the formation of low melting point copper rich phases that might cause fissured surfaces during rolling. The nickel remains with the copper during remelt cycles thus allowing scrap to be used in melts of other steels without any harmful effects [Ref. 4].

Chromium and molybdenum are added to retard auto-aging. This insures useful strength in heavy sections. The chromium also serves to improve the corrosion resistance of this steel. Tests have shown that this grade of steel develops a very tightly adherent rust film, making it more corrosion resistant than many other steels in a marine environment [Ref. 5].

Manganese increases the hardenability of the steel, but is kept in the 0.4 to 0.7 weight percent range to prevent possible embrittlement due to martensite formation at grain boundaries [Ref. 6].

Phosphorous is an impurity element present in the steel making process and its weight percent must be kept as low as possible to minimize the formation of brittle iron and nickel phosphides which lead to embrittlement [Ref. 7].

Sulfur is detrimental to notch toughness and is therefore kept to a minimum. Reduction in sulfur content is also a method of controlling a steel's susceptibility to lamellar tearing [Ref. 8].

During the steel making process silicon is used as a deoxidant. The amount of silicon must be kept low to minimize the number of silicates which promote cracking [Ref. 9].

C. INFLUENCE OF HEAT TREATMENT ON NICOP PROPERTIES

Two step heat treatments are required to obtain the desired strength and improve notch toughness. Austenitizing above the A_{c3} critical temperature is the first step in producing normalized (class 2) or quenched (class 3) plates. Temperatures of 900 to 925°C (1650-1700°F) should be used with adequate soak times. Normalized plates are then air cooled while class 3 plates are quenched in water.

Precipitation hardening is the second heat treatment step. This involves heating the steel to 540 to 700°C (1000 to 1300°F) followed by air cooling. This step allows copper particles to precipitate and increase strength. Time and temperature greatly influence strength as they change particle size, particle spacing and volume fraction.

D. WELDABILITY OF ASTM A710 GRADE A STEEL

Laboratory tests and field experience have shown this steel to be readily welded using any of the current welding methods [Refs. 10, 11]. Hot cracking has not been encountered even with copper of 1.0 to 1.3 percent. Specimens have been welded with dampened electrodes at -73°C (-100°F) without observing hydrogen-assisted cold cracking [Ref. 12].

E. SCOPE AND OBJECTIVE OF PRESENT WORK

The present research effort is part of a development program on high strength-low alloy steels for naval structural applications being conducted by David Taylor Naval Ship Research and Development Center. One phase of this program is to evaluate the weldability of selected candidate alloys. This research effort addressed the effects of preheat on shielded metal arc weldments of 19mm (3/4 inch) thick plates of Armco Steel Corporation's NICOP class 3 steel.

II. BACKGROUND

During the welding of steels, the base metal adjacent to the weld region is subjected to various peak temperatures and rates of heating and cooling. These temperature changes lead to changes in the microstructure of the base metal in the heat affected zone which can lead to problems in the welded structure. Two possible problem areas are hydrogen assisted cracking and reduction of toughness in the heat affected zone.

A. HYDROGEN CRACKING

Hydrogen assisted cracking occurs when the following four factors are present: hydrogen in the metal, a tensile stress, a temperature between -100 to 200°C (-150 to 390°F) and a crack-sensitive microstructure.

Hydrogen is introduced into the base metal from the atmosphere and moisture on the weld electrodes. Standard practice on welded high strength steel products has been both to pre and, in some cases, post-weld heat treat the welded region to both eliminate the source of hydrogen and to allow the hydrogen to diffuse out of the metal. The increase of welded structures used in harsh environments (Artic pipeline, North Sea oil platforms) lead to the requirement for a steel which can be economically produced and welded without elaborate pre and post-weld heat treatments.

The hardness level of a steel is an indication of its susceptibility to hydrogen cracking due to its microstructure. Bernard [Ref. 13] has shown that a DPH (diamond pyramid hardness) below 350 indicates that the region is at least partially non martensitic and that there is a linear relationship between carbon content and hardness (Figure 1). Using this approach is not completely satisfactory in assessing microalloyed steels for tendency toward hydrogen cracking as other alloy additions need to be considered.

Investigations into the role microalloying elements have on hydrogen assisted cracking are limited. The wide variation in compositions make interpretation of data difficult. It has been shown [Ref. 14] that alloy additions do not operate alone to affect changes in steel but work in conjunction with other additions to alter the steel's microstructure.

B. HEAT AFFECTED ZONE TOUGHNESS

Notch toughness is an important property of steel as an indication of how a steel will withstand an applied stress with a notch present. The notches can be sharp corners, cut outs, cracks introduced during welding or other defects which act as stress concentrators. In a welded structure it is desired to have the notch toughness in the weld metal and heat affected zone as high as that in the base metal.

Microstructure has a pronounced affect on the toughness of steels and the microstructures in the HAZ are dependent

on the weld process and the welding parameters including; peak temperatures reached, cooling rate, alloy content and non-metallic content. As stated previously, the higher the carbon content, the more brittle the transformed structure. The most intrinsically brittle structure found in steel is high carbon twinned martensite. To improve toughness for a given martensite content, reduction of the width of the martensite is required. In a low carbon, low alloy steel, such as NICOP, it is possible to improve notch toughness through the formation of auto tempered martensite. This is a low carbon martensite which forms at a high temperature and tempering occurs during the cooling to room temperature [Ref. 15].

C. PREVIOUS STUDIES

Studies on the weldability of steels having the composition of NICOP are limited. The work that has been presented in the literature deals mainly with notch toughness and other mechanical properties. Metallography of welded structures of NICOP has been limited to optical microscopy and some scanning electron microscopy. The transmission electron microscope has only been used to examine the clusters of epsilon copper in the base metal.

Redfern and Minard [Ref. 16] reported the results of the first stage of an on-going program studying the weldability of a Ni-Cu-Cb-Cr-Mo steel. The work examined the steel's

resistance to hot and cold cracking during welding. The Gleeble hot ductility test was utilized to simulate the thermal cycle close to a weld deposit in 12mm (1/2 inch) plate welded with an energy input of 2 KJ/mm (50 KJ/in). The steel maintained a very high ductility on heating to and cooling from temperatures close to its melting point. This indicates that the steel is not susceptible to hot cracking.

Two sets of 32mm (1-1/4 inch) plates were welded using damp electrodes to increase any tendency towards hydrogen cracking. One set was manually welded with the plates held at -73°C (-100°F). The frost that formed over the weldment was brushed away before laying down the next bead and no attempt was made to dry the surface. In both cases no cracking was observed in the HAZ or the base metal. A bend specimen taken from the HAZ was bent without cracking.

Neither pre nor post-weld heat treatments were used for making any of the test welds. X-ray inspection of the 12mm (1/2 inch) plate and 19mm (3/4 inch) plate welds showed them to be sound. No incident of hot or cold cracking was found in examining the base plate.

An investigation into the effects of energy input, plate thickness, base metal heat treatment and post weld stress relieving on heat affected zone toughness of submerged arc weldments made in NICOP steel show good results [Ref. 17].

Heat affected zone toughness decreases as weld energy input increased in 9.5mm, 19mm and 57mm (3/8, 3/4 and 2-1/4 inch) thick plates. The Charpy V-notch energy was over 27 joules (20 ft-lbs) at -46°C (-50°F) for all welds. This indicates that this alloy may be readily welded with high deposition rates. Maximum weld energy input rates were 3 KJ/mm (75 KJ/in) for 9.5mm (3/8 inch), and 5 KJ/mm (125 KJ/in) for 19mm (3/4 inch) and 57mm (2-1/4 inch) plates.

All three classes of ASTM A710 grade A alloy steel maintain good HAZ toughness in the as-welded condition. Over 68 joules (50 ft-lbs) of energy at -46°C (-50°F) was provided by all heat treatment classes of 19mm (3/4 inch) thick plate welded with 2 KJ/mm (50 KJ/in).

The toughness of the weld metal and HAZ was lowered by stress relieving at 565°C (1050°F). The reduction in toughness occurred due to precipitation strengthening which occurred. This strengthening was confirmed by an increase in peak hardness.

The as-welded condition of all samples produced a maximum hardness of 25 to 28 HRC in the heat affected zone. This hardness is below that usually associated with hydrogen assisted cracking and thus eliminates a requirement to stress relieve.

III. EXPERIMENTAL PROCEDURE

A. MATERIAL

A 19mm (3/4 inch) thick plate of NICOP class 3 alloy steel was provided by Armco Steel Corporation's Houston, Texas plant to David Taylor Research and Development Center. The plate, from heat number 48259, was austenitized at 899°C (1650°F) for forty-five minutes and water quenched. Following the water quench the plate was precipitation hardened at 594°C (1100°F) for thirty minutes and air cooled. The chemical composition and tensile mechanical properties are presented in Tables I and II.

Sections of the plate were cut for fabricating the two shielded metal arc weld samples at David Taylor Research and Development Center. Electrode type MIL-11018-M, conforming to MIL-E-22200/1E, 3/16 inch diameter, HT 8413719, lot number A 704G11A were used to make both weldments. Electrode chemical composition is given in Table III [Ref. 19]. Joint design was a sixty degree double-V groove with a 3mm (1/8 inch) root gap. Samples were welded per specification (Table IV) to produce a finished plate measuring 305mm (12 inches) by 305mm (12 inches). Finished welded samples were sent to the Naval Postgraduate School for examination.

B. SAMPLE PREPARATION

Traverse cuts were made in the plates to produce sections for examination. The sections were taken 38mm (1.5 inches) from the end of the plates to minimize any effects from starting or stopping a weld pass. A macro etchant solution was prepared using 2 percent Nital solution (nitric acid (HNO_3) and ethanol (C_2H_5OH) which revealed the weld area, heat affected zone and base metal. A section 25.2mm (1 inch) in length, containing the weld metal, HAZ and base metal, was cut from each section using a Buehler cut-off machine. Standard metallographic techniques were employed to provide a surface which was optically flat at 600x. The specimens were etched to reveal the welded region, fusion line, HAZ and base metal. The location and number of weld passes was verified on both specimens.

C. MICROHARDNESS MEASUREMENTS

Three microhardness traverses were performed on each sample. The traverses were taken on the side having two weld passes (Figures 2 and 3). One traverse crossed the HAZ produced by the first weld pass and across the first weld pass. The second traverse mapped the HAZ and weld metal region which was reheated by a subsequent weld pass. Traverse three provided a map of the HAZ and weld metal which was produced by the final weld pass on the side. The traverses provided a comparison of hardness between the preheated and non-preheated samples.

A Buehler microhardness tester, using a diamond pyramid indentor, 200 gram load, 600X optical system was utilized to make the microhardness measurements. Adequate spacing was taken between measurements to permit accurate determination of the slope of any hardness gradient.

D. OPTICAL MICROSCOPY

A Zeiss Universal Research Microscope was used to examine and record the microstructure at magnifications of 16X to 200X. A 2% Nital solution was employed to reveal the microstructures. The three regions traversed during the microhardness measurements were fully examined and compared.

E. SCANNING ELECTRON MICROSCOPY

Micrographs at 2300X were taken across the region of the second microhardness traverse to obtain a visual map of the microstructure. The micrometer on the scanning electron microscope (SEM) was used to locate the distance from the fusion line at which the photographs were taken. Foils examined with the transmission electron microscope were etched and re-examined with the SEM. The microstructure of the foil was compared to those from the traverse of the region to confirm the exact location of the foil. The SEM work was done with a Cambridge Stereo Scan S4-10.

F. WAFERING OF MATERIAL ALONG THE HAZ

The preparation of foils for transmission electron microscopy required careful work so that distances from the fusion

line were accurately known. The initial step in this process is the slicing of the sample into thin wafers. The samples were first cut in such a manner that the area containing weld metal, HAZ and base material previously examined could be mounted in an ISOMET Low Speed Wafering machine. The samples were mounted with the fusion line parallel to the low concentration diamond cut-off wheel. The base, HAZ and weld metal regions were wafered into 0.25mm (0.01 inch) nominal thickness slices. A detailed accounting system was maintained during wafering. First, the micrometric feed assembly kept track of the saw blade in relation to the fusion line. Additionally the sample's thickness was measured and recorded prior to and after each slice to determine loss of material due to the blade thickness.

G. THIN FOIL PREPARATION

For proper transmission electron microscope (TEM) work the preparation of thin foils of NICOP alloy steel was essential. It is necessary that the volume of NICOP steel material be kept to a minimum to avoid astigmatism (interference) of the electron beam due to the magnetic fields generated from the specimen when placed in the electromagnetic fields inside the electron microscope.

After the regions to be examined were selected the wafers were thinned manually to a nominal thickness of 0.16mm (0.006 inch). Care was taken during this step to keep the wafer flat

and not bend it in any way. Disks 3mm in diameter were punched for additional thinning with a Struers Tenupol and Streuers Polipower apparatus. The electrolyte, consisting of 10% percloric acid ($HClO_4$) and 90% methanal (CH_3OH) was maintained at a temperature of -45°C (-49°F). The Polipower was set at 17 volts and a current of 40 milliamps. A medium flowrate setting on the Tenupol was used in conjunction with the sensitivity of the photo cell circuit adjusted to terminate electropolishing upon initial penetration.

H. OBSERVATION IN THE TRANSMISSION ELECTRON MICROSCOPE

A JEOL JEM-120CX MK II transmission electron microscope (TEM) was used to examine the NICOP thin foils. An accelerating voltage of 120 kilovolts was used during all foil observations. Reproducibility of the foil preparation technique allowed foils from all areas being investigated to be examined at from 10000X to 67000X. Selected areas were examined at higher magnifications.

IV. RESULTS

A. MICROHARDNESS TRAVERSES

Comparison of traverses taken across the preheated and non-preheated sample in Figures 4, 5, and 6 show the curves to be nearly identical. In all cases, the hardness gradient in the HAZ of the preheated sample has a slightly steeper slope, i.e., the same hardness change occurs over a smaller distance. Figure 7 shows how the hardness gradients of the three traverses of each weldment nearly overlay each other. A softening of about 20 DPH (diamond pyramid hardness) in the region just inside the HAZ/base interface was observed in all cases. All hardness curves show a steady increase in hardness from the softened region to a maximum hardness in the weld metal. A maximum hardness of 310 DPH was recorded in the weld metal, hardness of about 240 DPH at the fusion line and minimum hardness of 172 DPH was observed in the HAZ just inside the HAZ/base metal interface. The base material of both samples had a nominal hardness of 220 DPH Table V lists the maximum and minimum readings recorded during each traverse.

B. GENERAL OPTICAL OBSERVATIONS

Optical microscopy of the HAZ region at the fusion line revealed that the grain size decreased across the HAZ as the distance from the fusion line increased. The microstructure

of the coarse grain HAZ region, adjacent to the fusion line, produced by the root weld pass, contains three distinct grain areas. In the lower portion of Figure 8 there is an area in the coarse grain region where grain boundaries have a net-like structure [Ref. 18] adjacent to the visible HAZ which results from the second weld pass. Near the center of this coarse grained HAZ of the root pass is the visible HAZ from weld pass 3. The grain boundaries in this area also have a net-like structure (Figure 8). The peak temperatures subsequent to the root pass created by passes 2 and 3 (Figure 2) in this location would be in the intercritical temperature range, providing a partial austenitization. In the area between these two visible heat affected zones the peak temperatures from passes 2 and 3 would be below the A_1 and thus reaustenitization would not occur and the net-like structure did not form. The fine grain region in the visible HAZ of weld pass 3 is the result of this area reaching a sufficiently high peak temperature to fully transform to austenite prior to cooling. Both preheated and non-preheated welds had areas containing this net-like structure. The size of the area observed in the preheated sample was larger than in the non-preheated sample because the preheating broadens the temperature profile in the HAZ. Figure 9 illustrates this net-like structure located at the bottom edge of Figure 8.

C. BASE METAL

The base metal of both samples appeared to be predominately very fine grained polygonal ferrites (Figures 10 and 11). The fineness of the grain size prevented a determination of the grain size with the optical microscope. Scanning electron microscope examination revealed the ferrite grain size to be approximately 6 microns and also the presence of small islands of a second phase constituent as shown in Figures 12 and 13. The TEM examination revealed a high dislocation density and a fine epsilon copper precipitate in the ferrite. Small regions of tempered martensite and ferrite/carbide aggregates were observed along the ferrite grain and subgrain boundaries, Figures 14 and 15. The islands of second phase constituents observed in the SEM appear to be these regions of tempered martensite and the carbide/ferrite aggregates. The preheated and non-preheated samples both possessed these structures.

D. HAZ/BASE REGION

It was difficult to clearly define the start of the HAZ/base metal interface. Increasing the etching time of the specimens such that the other regions were over etched helped to more clearly locate the start of the HAZ. This area showed a structure similar to that of the base material of both samples. The SEM revealed the nominal ferrite grain size in this region to be slightly larger than that of the base region (Figures 16 and 17). TEM examination revealed fewer islands

of tempered martensite and carbide/ferrite aggregates in this region as compared to the base metal (Figures 18 and 19). However, these differences are believed to be due to the variation in microstructure of the base metal not due to welding. The dislocation density and epsilon copper distribution was similar to that observed in the parent material.

E. HAZ AT FUSION LINE

The grain boundaries in this region appear to be decorated by a different microconstituent, resulting when a subsequent weld pass heats this region into the intercritical temperature range. The area with this effect was larger in the preheated sample than in the non-preheated sample. At low magnification it appears as a net-like structure surrounding the ferrite grains and at higher magnification separate particles are revealed. SEM observations in this region revealed the net-like structure, previously described, to be a second microconstituent on the grain boundaries (Figure 20). The area adjacent to these grain boundaries were free of second phase particles (Figure 20, SEM micrograph C). SEM microscopy (Figures 21 and 22) of the TEM foils examined from this region of the HAZ reveal their microstructure to be similar to that observed within the grain shown in Figure 20. X-ray dot map and line scan analysis using a Princeton Gamma Tech 1000 were performed in an attempt to identify these particles. Within the limits of the equipment available no copper or other alloying element segregation has occurred.

Regions believed to contain the net-like structure discussed above appeared to be islands of auto tempered martensite and ferrite/carbide aggregates when observed by TEM (Figures 23 and 24). In some areas a region of martensite and/or ferrite/carbide aggregate exists between the ferrite laths, Figure 25. This morphology appears to be that which was observed in Figure 20. The number of tempered martensite islands and ferrite/carbide aggregates in this region is greater than the number observed at the HAZ/base interface. (Figures 16 and 17) The carbon content of these regions appears to be much higher than the 0.04 percent bulk carbon of the material. In some instances, Figure 23a, this has led to the formation of transformation twins in the martensite. The overall microstructure was lath-like in this region. In both samples there were areas of carbon free ferrite laths with retained austenite at the lath interface, Figure 23. The number density of epsilon copper precipitates observed in the base metal, Figures 14 and 15, was reduced significantly.

F. MIXED REGION

This region had a much finer microstructure than the adjacent HAZ region (Figure 26). Both samples possess numerous islands of the second microconstituent in this location. The grain boundaries appear to be free of this second microconstituent except in isolated areas. Small inclusions are present throughout this region. TEM examination revealed

lath martensite which had been tempered by the subsequent adjacent weld pass, patches of retained austenite located at some of the lath interfaces polygonal and carbon free ferrite laths. The preheated and the non-preheated weldments both possess similar microstructures (Figures 27 and 28).

G. WELD METAL

SEM observations revealed a similar microstructure in the preheated and the non-preheated samples, Figure 29. TEM examination of the weld metal at the center of the weld revealed the same microstructures as those observed in the mixed region, however, the dislocation density is higher and more inclusions are present than in the mixed region, Figures 30 and 31.

V. DISCUSSION OF RESULTS

A. COMPARISON OF MICROHARDNESS PLOTS

The softened region observed with all microhardness traverses is most likely the result of over aging. This region has been reported in submerged arc weldments of similar material in similar plate thickness [Ref. 20]. Tension tests, conducted by Jesseman and Schmid, showed that no adverse affects to joint strength was produced by this softened region. They note that higher energy inputs increase the size of this softened region and therefore may be of concern in electroslag or electrogas welding.

The similarity in slopes from this softened region to the fusion line of traverses A, B, and C plus traverses A', B', and C' is caused by the general increase in second micro-constituents (tempered high carbon bainite/martensite) as the distance from the fusion line is decreased. Had this increase in hardness been a result of tempering or precipitation hardening, the hardness traverse in the last weld pass region (C and C' respectively) would have been different from that observed in the previous two passes as the final weld pass was not reheated.

B. NICOP BASE METAL

The microstructure observed in the parent material adjacent to the HAZ was typical of the microstructures in NICOP

class 3 alloy steel. The rapid rate of cooling from the austenitizing temperature, during the fabrication process, prevents the formation of pearlite in class 3 plates, and causes a fine grained polygonal and acicular ferrite to form with some islands of bainite and martensite. The subsequent precipitation hardening allows the epsilon-copper to appear. As the preheat temperature of 121°C (250°F) is well below the A_1 temperature and the 650°C aging temperature no change in microsturcture between samples was expected or observed.

C. HAZ ADJACENT TO VISIBLE HAZ/BASE INTERFACE

In this location the peak temperature reached was in the vicinity of the A_1 temperature for this alloy [Ref. 21]. The time in this temperature range appears to have caused some over aging to occur producing the softened region in the microhardness traverses. The distance from the fusion line to this area is greater in the preheated sample than in the non-preheated sample, since preheat spreads the temperature profile during welding over a greater distance.

D. HAZ ADJACENT TO FUSION LINE

The peak temperature in this HAZ near the fusion line is near the melting point of NICOP steel. This temperature allows complete austenization of the region to take place, however, the increase in the number of second microconstituent islands (high carbon bainite, martensite and ferrite/carbide aggregates) indicates that some chemical inhomogeneities exist.

Shackleton [Ref. 22] reported that at high temperatures copper may melt and then penetrate along the grain boundaries resulting in premature failure when the steel is subsequently stressed. This adverse effect copper has when it "wets" the grain boundaries was one of the reasons for care in examining the grain boundaries in this region. The X-ray dot map and line scan of the region failed to reveal the presence of any segregation of copper.

The most logical cause of this net-like structure is that during the thermal cycle from the first weld pass a lath structure is formed on cooling with some retained austenite at the lath interfaces. From a subsequent weld pass the peak temperature is only in the intercritical temperature range causing partial austenitization. This partial austenitization causes austenite to nucleate at lath interfaces and prior austenite grain boundaries. Austenite along the grain boundaries transforms to a higher carbon martensite on cooling.

Koso, et al, [Ref. 23] in a study of narrow-gap welds in a HSLA steel containing 0.1 weight percent carbon, reported similar grain boundary structures which they termed net-like structures. Koso concluded that this net-like structure consisted of high carbon martensite islands based on the observation of fine transformation twins within the martensite grains.

TEM observations of this area in NICOP steel revealed twins within the martensite grains, but only infrequently. The martensite islands observed had the appearance of tempered

martensite and frequently appeared as ferrite/carbide aggregates. These islands are the components of the net-like structure in this region of the NICOP weldments examined and are also the second microconstituent observed throughout the heat affected zone.

E. MIXED REGION AND WELD METAL

The initial microstructure in the weld metal is a result of solidification and cooling. Any subsequent weld passes serve to temper this initial structure. During the fabrication of the two weldments all welding parameters were kept as nearly identical as possible, except for the preheat temperature. The cooling rate was the only difference between the two samples. The peak temperatures reached, in the regions examined, were similar because heat input and travel speed were the same in both cases. This observer was unable to detect any difference in the weld metal microstructure at the weld pool center or in the mixed region when comparing the preheated and the non-preheated samples. The continued increase in hardness from the fusion line into the weld metal is probably due to the increasing carbon content from the NICOP to the undiluted weld metal.

F. COMMENTS ON HYDROGEN ASSISTED CRACKING SUSCEPTIBILITY (HAC)

Since the HAZ hardness never exceeds 260 DPH hydrogen assisted cracking is not expected [Ref. 24]. The higher carbon content islands in the base metal, which increased in numbers

in the HAZ, will probably have some hydrogen cracking susceptibility. However, the fact that they are islands surrounded by microstructures that are not expected to be susceptible will minimize this effect and no significant problem with HAC is expected. Both preheated and non-preheated welds contained the islands and thus, from a microstructural view point, the HAC susceptibility would be expected to be similar. There are, however, other considerations that must be made before preheating is eliminated, the most important being the effect on the weldment hydrogen content.

G. NOTCH TOUGHNESS

The microstructure observed in the HAZ should have good notch toughness and no effect of preheat would be expected. Previous work on submerged arc welds [Ref. 25] indicated that the HAZ CVN toughness was the same in both the fine and coarse grained regions of the HAZ. The lowest toughness was located in the weld metal (AWS EM2).

VI. CONCLUSIONS

1. Similar locations relative to the fusion line (e.g. HAZ/base metal interface) in the preheated and the non-preheated samples exhibit the same microstructures.

2. The only discernable effect of preheating to 120°C vs cooling to -1°C is to widen the HAZ by about 1mm.

3. The low carbon content of NICOP results in the formation of low carbon lath ferrite in the HAZ. However, islands of a higher carbon content microconstituent were found and they increase in number density as the fusion line is approached. This results in an increase in hardness of about 20 DPH over that of the as-received base metal.

4. The hardness from the fusion line into the weld metal increased by about 50 DPH due to mixing of the weld metal with the NICOP in this region.

5. From the point of view of HAZ microstructure NICOP can be welded without preheating as hydrogen assisted cracking is not expected to be a problem in the HAZ.

VII. FUTURE WORK

1. More research into the origin and composition of the "islands" observed should be preformed.

TABLES

TABLE I

Chemical Composition of NICOP Alloy Steel

Alloy		Weight Percent
Carbon	.....	0.04
Manganese	.....	0.51
Chromium	.....	0.68
Nickel	.....	0.93
Molybdenum	.....	0.20
Copper	.....	1.20
Columbium	.....	0.042
Phosphous	.....	0.01
Sulfur	.....	0.009
Silicon	.....	0.31

TABLE II

Tensile Mechanical Properties

	0.2% Offset YS		UTS		Elongation % in 2 "	RA (%)
	(MPa)	(KSI)	(MPa)	(KSI)		
19mm longitudinal	592	89.5	701	101.7	27.5	74.5
19mm transverse	601	87.2	699	101.5	27.0	69.7

TABLE III

Chemical Composition of Electrode MIL-11018-M

Alloy		Weight Percent
Carbon	.....	0.10 max
Mangenese	.....	1.30 to 1.80
Silicon	.....	0.60 max
Phosphorus	.....	0.030 max
Sulfur	.....	0.030 max
Chromium	.....	0.40 max
Nickel	.....	1.25 to 2.50
Molybdenum	.....	0.25 to 0.50
Vanadium	.....	0.05 max

TABLE IV

Welding Specifications

	Preheat Sample	Non-preheat Sample
Preheat temperature	120°C (250°F)	-1°C (30°F)
Interpass temperature	107 to 135°C (225 to 275°F)	-1 to 3°C (30 to 37°F)
Voltage	22	22 volts
Amperage	190	190 amps
Travel speed	2.3 5.5 inch/min	2.3 mm/sec 5.5 inch/min
Heat input	2 KJ/mm (50 KJ/inch)	2 KJ/mm (50 KJ/inch)
Number of passes	5	5

TABLE V

Maximum and Minimum Microhardness Readings

Traverse	Hardness (DPH) MAX	MIN
Preheated sample		
A	285	187
B	286	185
C	289	185
Non-preheated sample		
A'	309	181
B'	310	190
C'	310	172

FIGURES

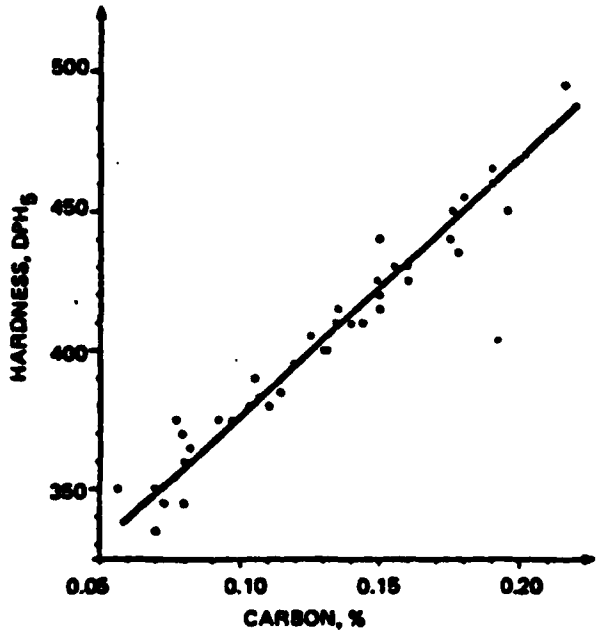

Figure 1. Effect of Carbon on Martensitic Hardness of Heat-Affected Zone for 41 Steels Tested. [Ref. 1]

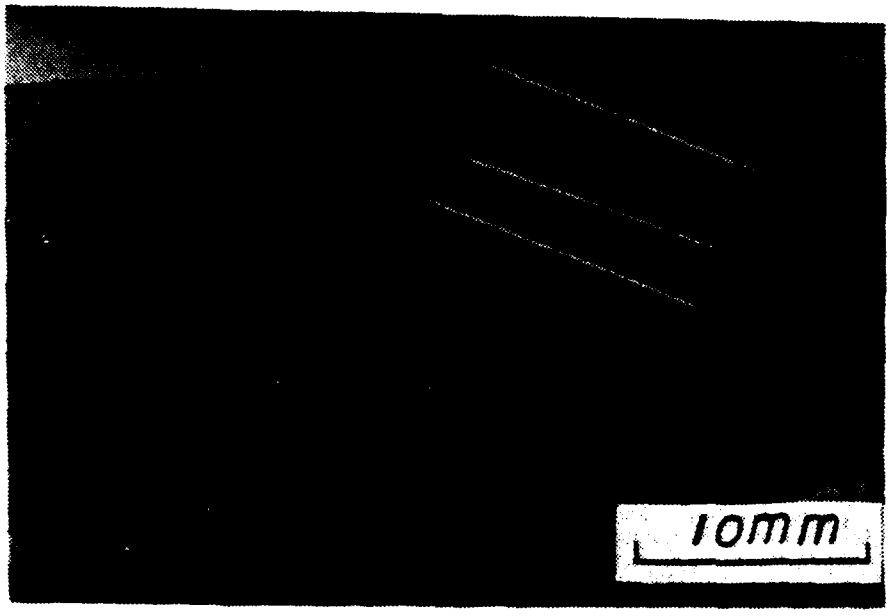

Figure 2. Locations of Microhardness Traverses on Preheated Weldment.

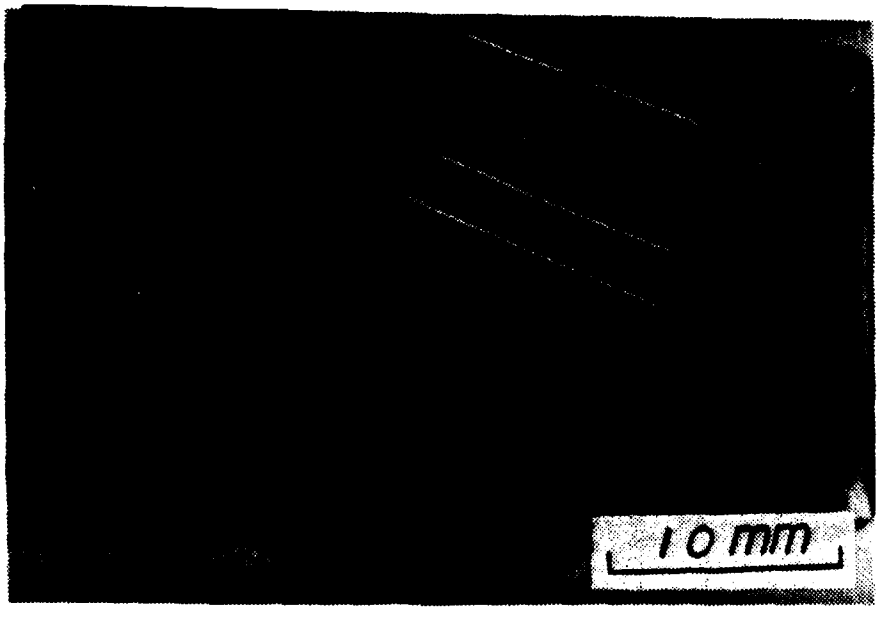

Figure 3. Locations of Microhardness Traverses on Non-Preheated Weldment.

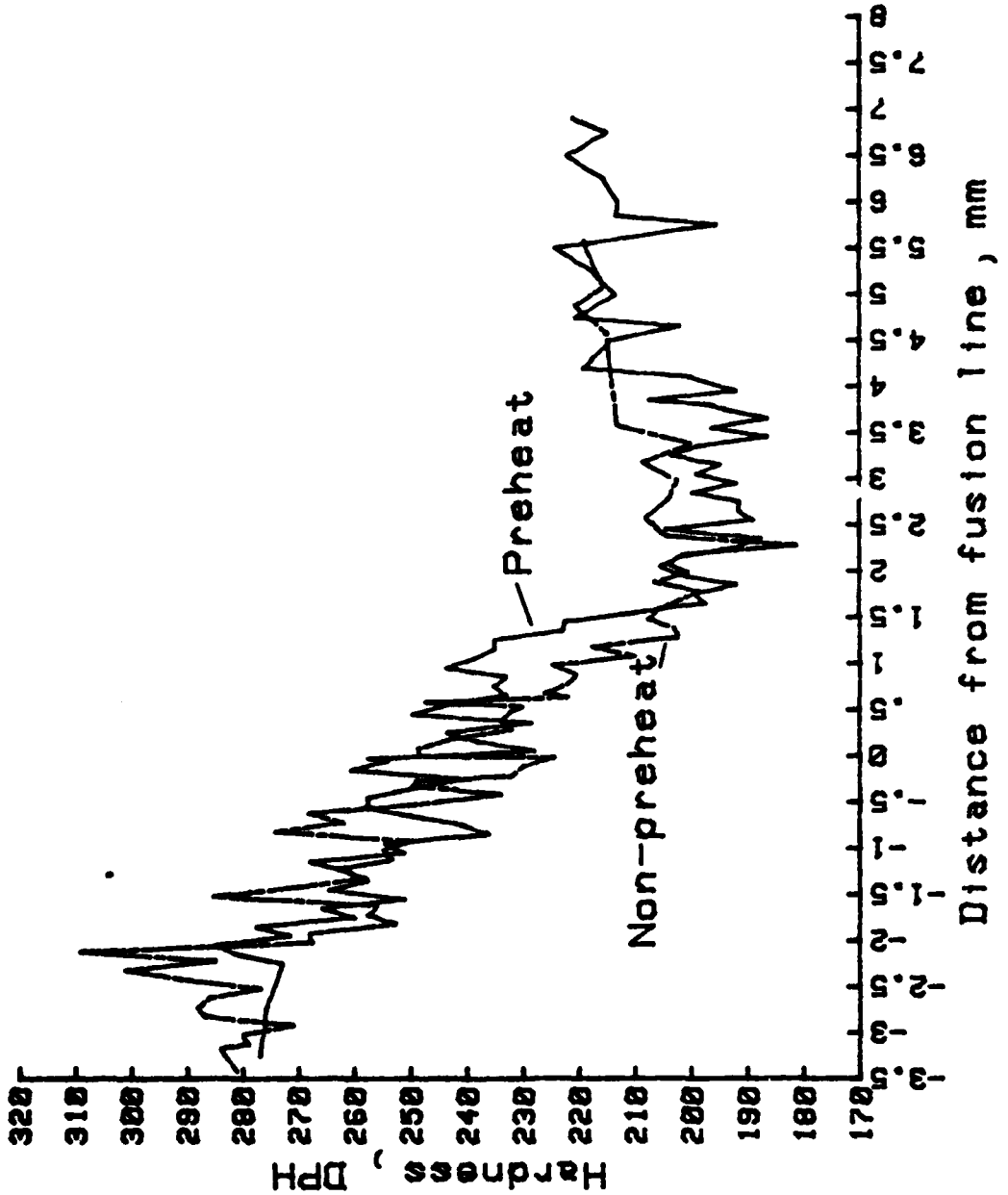

Figure 4. Comparison of Microhardness Traverses Across HAZ Produced by the Root Pass.

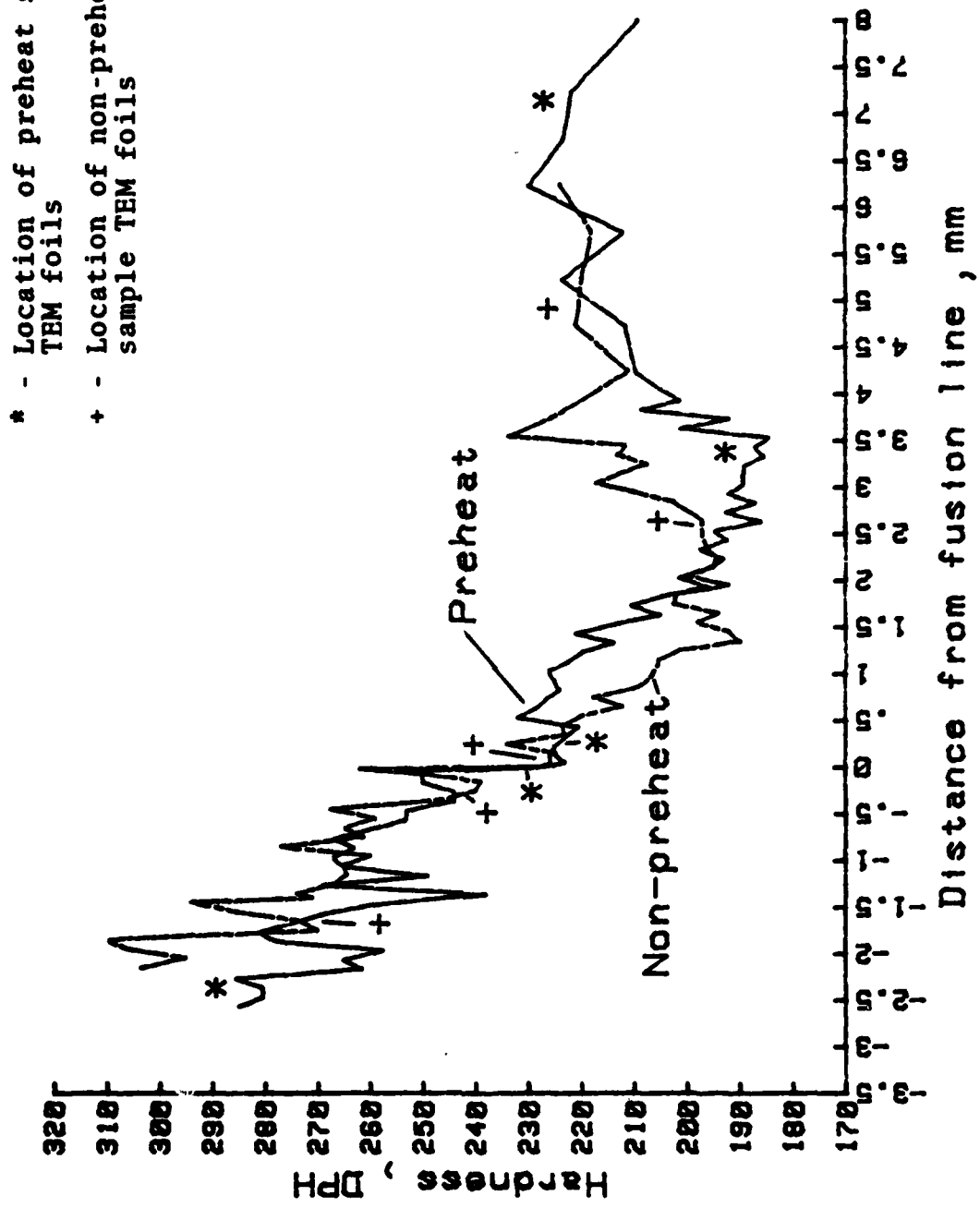

Figure 5. Comparison of Microhardness Traverses Across HAZ Region Reheated by a Subsequent Weld Pass.

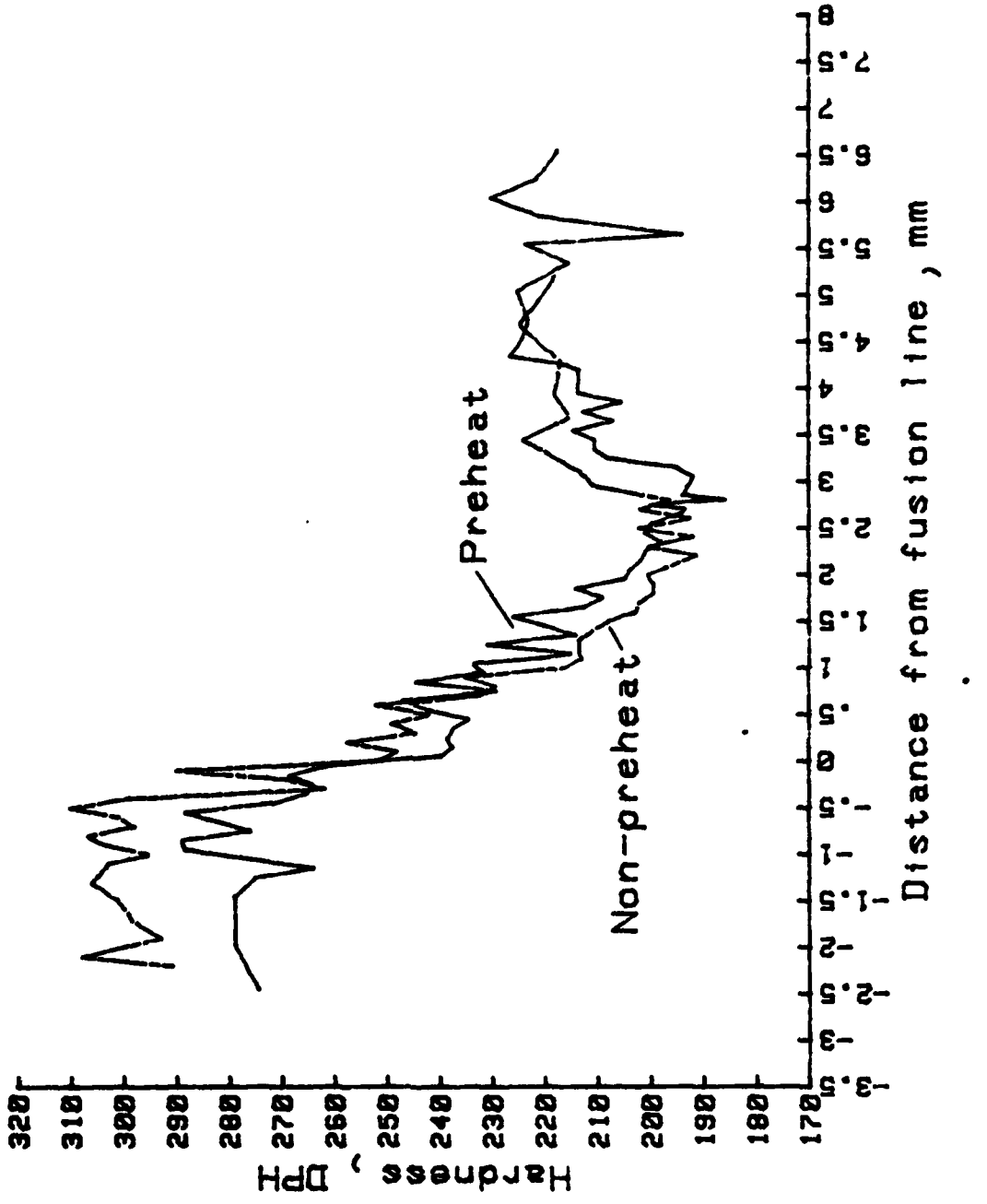

Figure 6. Comparison of Microhardness Traverses Across HAZ Produced by the Final Weld Pass.

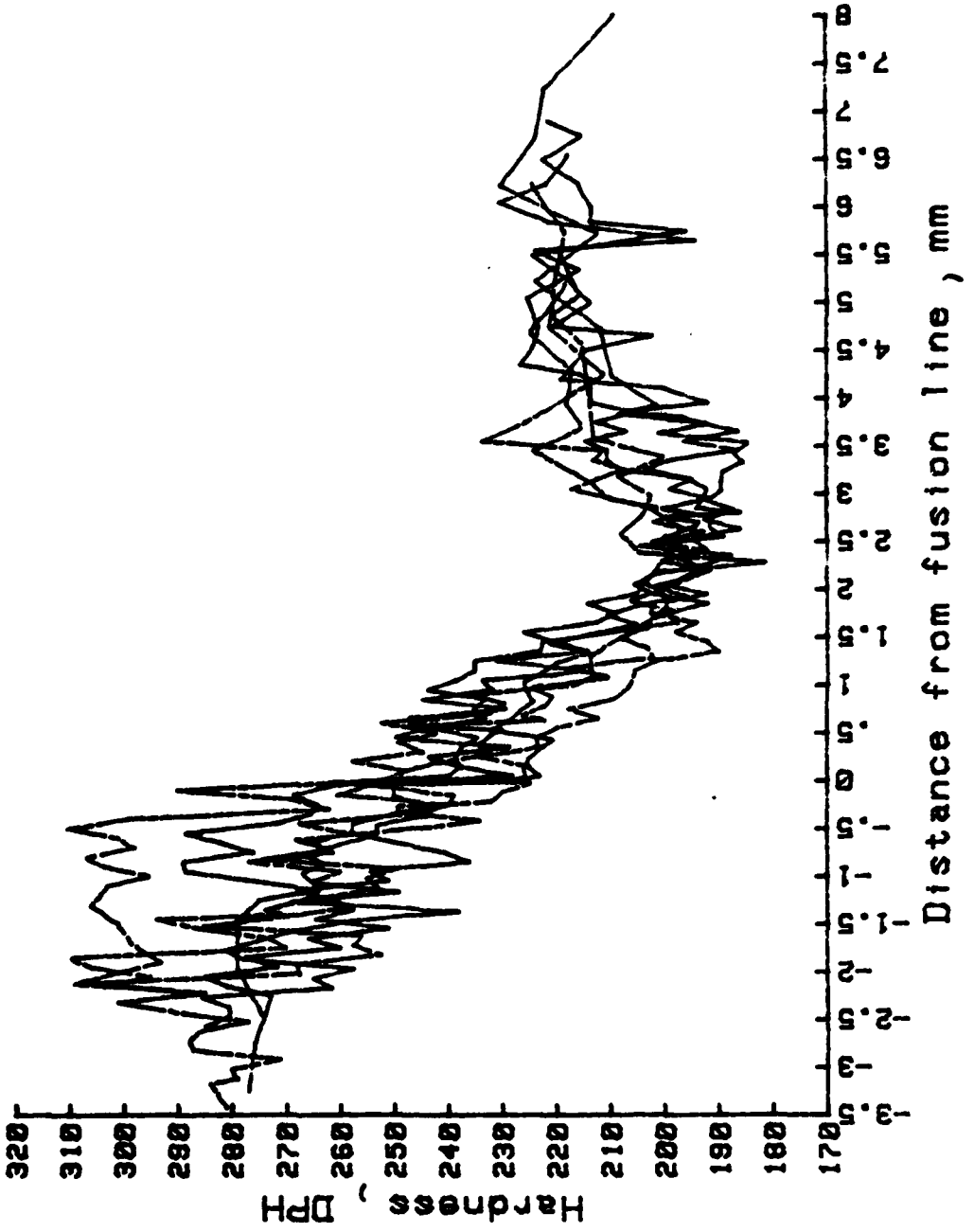

Figure 7. Overlay of the Six Microhardness Traverses Revealing the Similarity of the Curves Shown in Figures 4, 5, and 6.

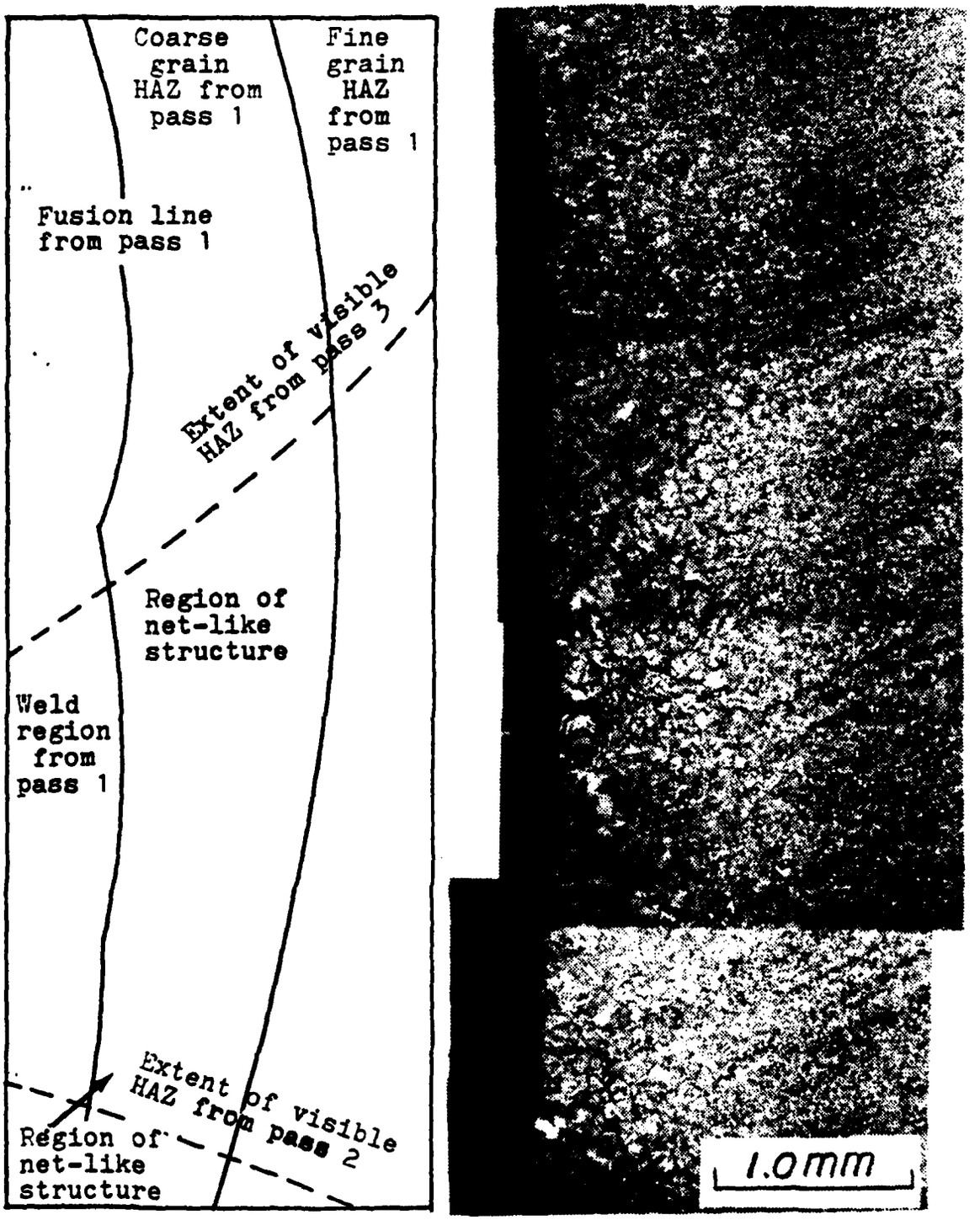

Figure 8. Microstructure of HAZ Adjacent to Fusion Line Showing the Effect of Subsequent Weld Passes.

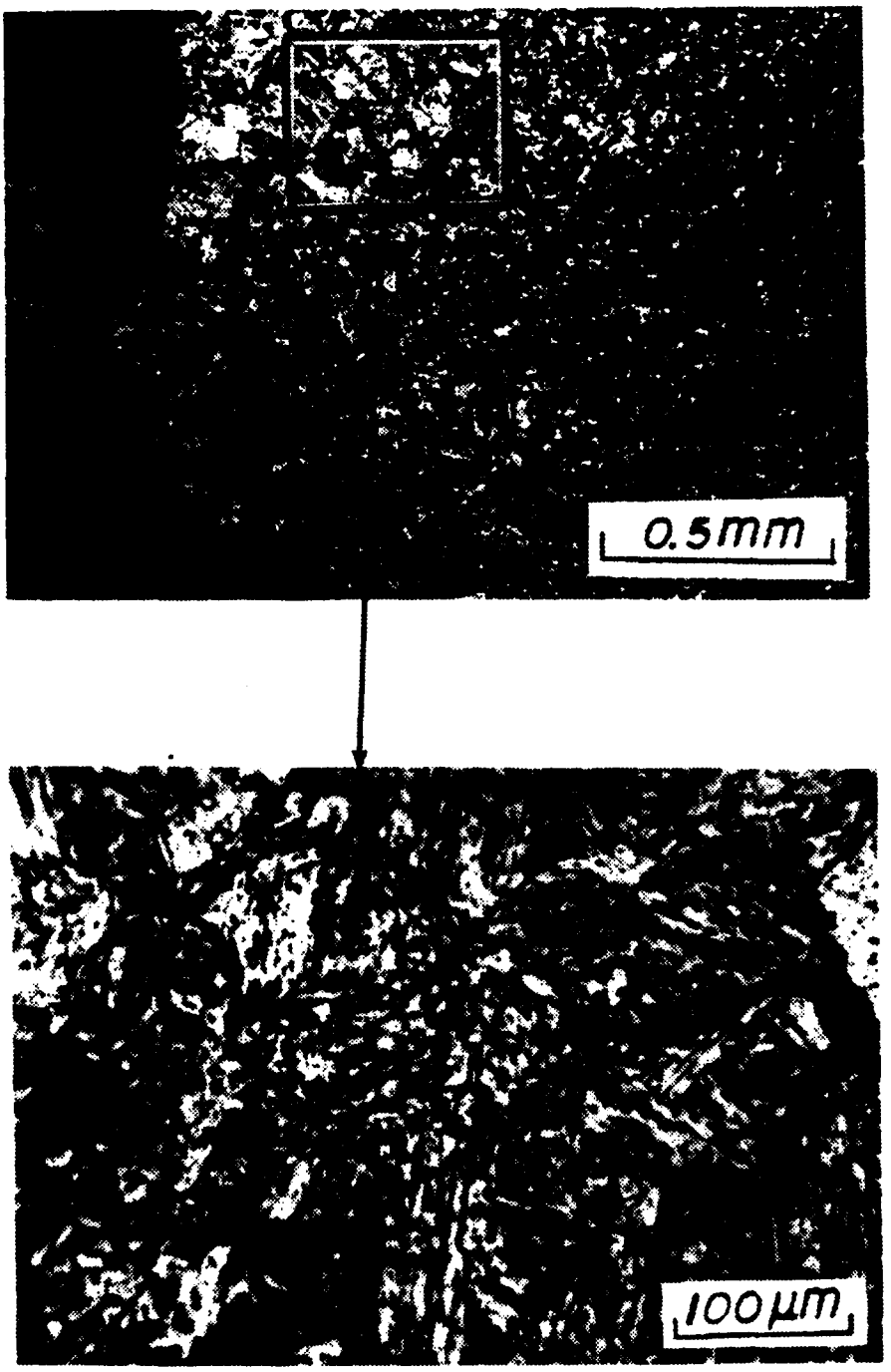

Figure 9. Region of HAZ Where Net-Like Structure was Observed in Figure 8.

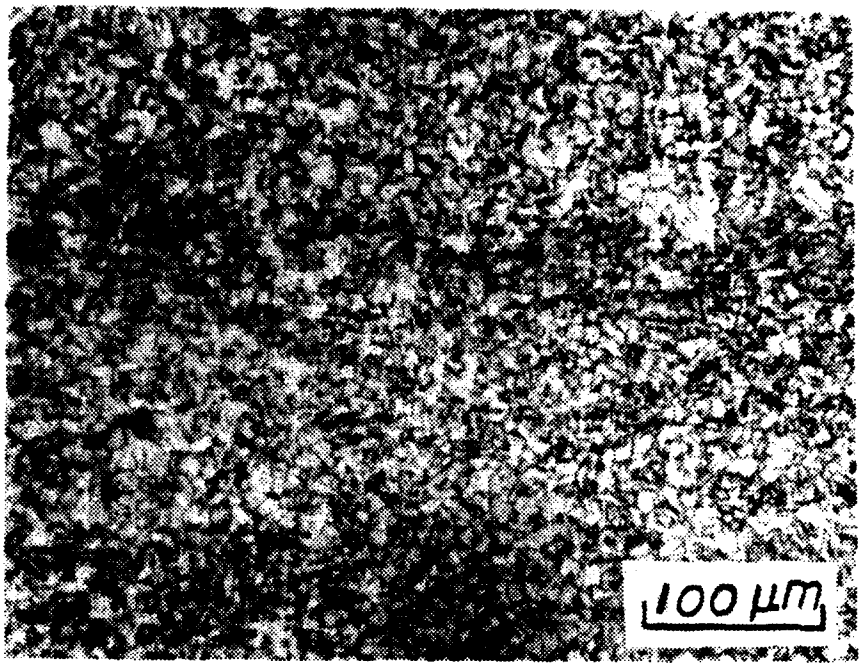

Figure 10. Typical Fine Grained Acicular and Polygonal Ferrite of Base Material in Preheated Weldment.

Figure 11. Typical Fine Grained Acicular and Polygonal Ferrite of Base Material in Non-Preheated Weldments.

Figure 12. SEM Micrograph of TEM Foil from Base Material in Preheated Sample.

Figure 13. SEM Micrograph of TEM Foil of Base Material in Non-Preheated Sample.

Figure 14. TEM Micrograph of Preheated Weldment Base Material.
A.) Dislocations and Fine Precipitates in Ferrite Grains.
B.) Ferrite/Carbide (FC) Aggregates and Ferrite Grains with Dislocations and Fine Precipitates.

Figure 15. TEM Micrographs of Non-Preheated Weldment Base Material.
A.) Dispersion of Fine Precipitate in Polygonal Ferrite. Dark Area in Upper Center is Carbide/ Ferrite Aggregate.
B.) Dislocation and Fine Precipitate in Fine Ferrite Grains.

Figure 16. SEM Micrograph of TEM Foil Preheated Sample's HAZ/Base Region.

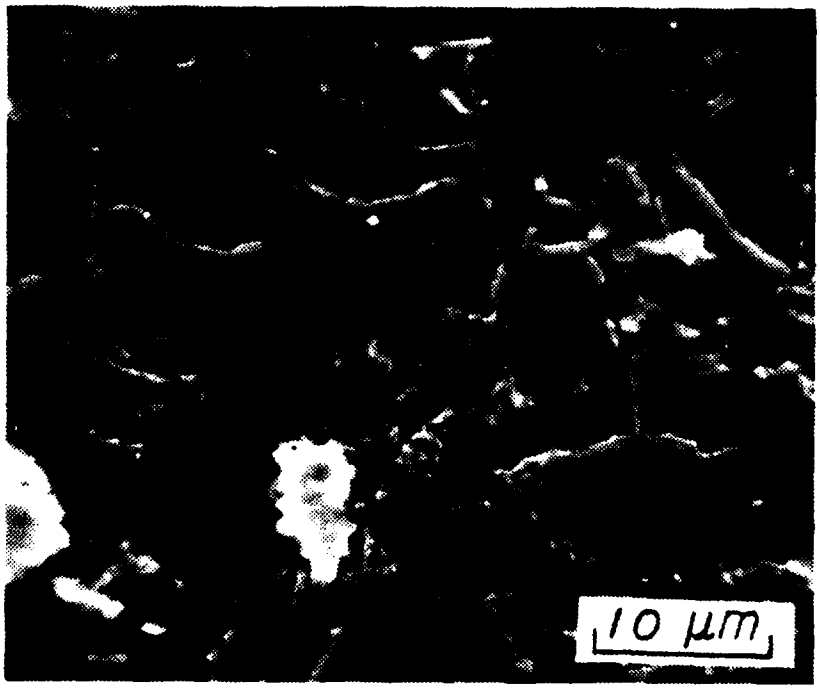

Figure 17. SEM Micrograph of TEM HAZ/Base Region in Non-Preheated Sample. White Appearing Particles are Artifacts due to Sample Contamination.

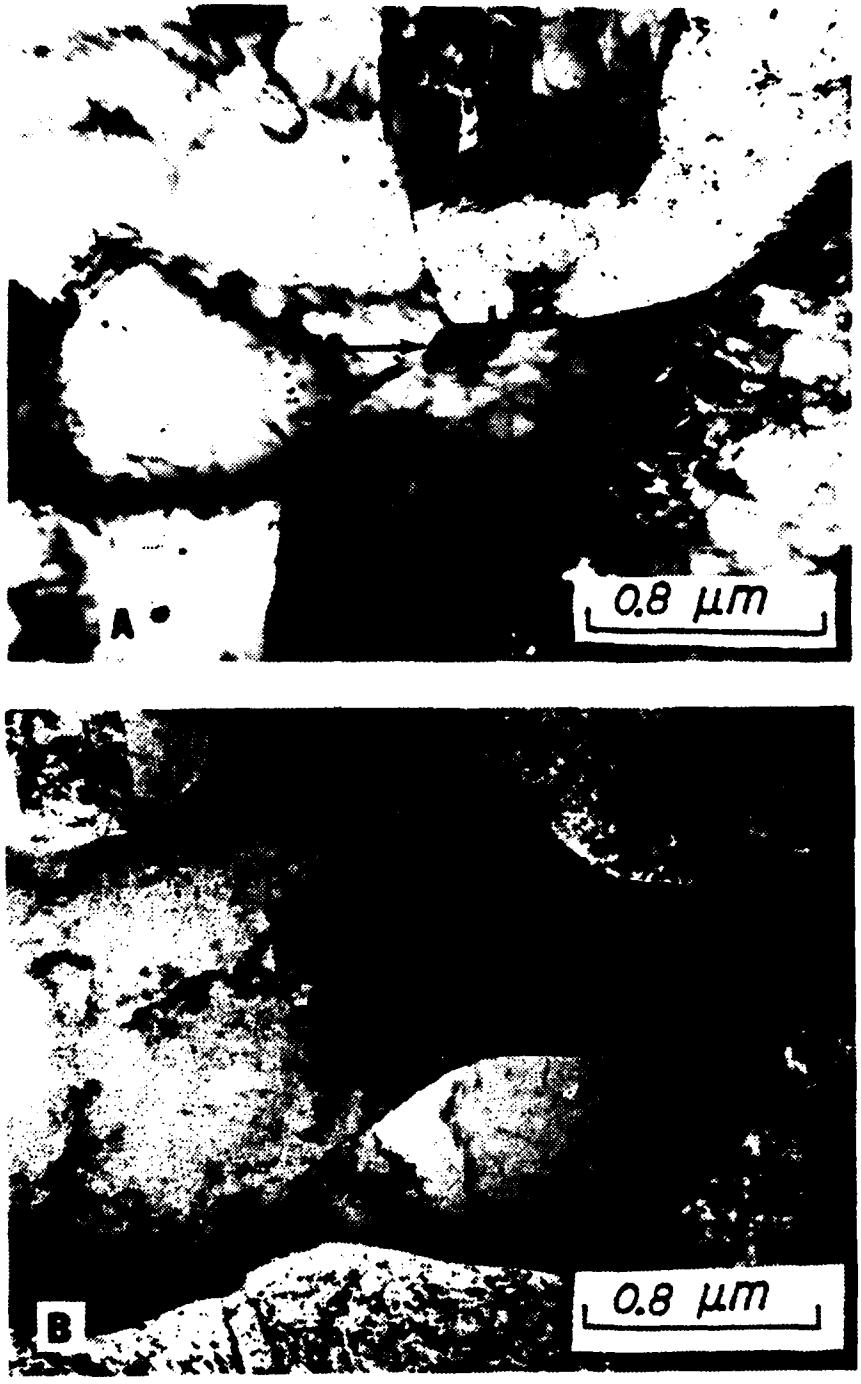

Figure 18. TEM Micrograph of Preheated Sample HAZ/Base Region.
A.) Fine Precipitate in Dislocated Polygonal Ferrite and Patch of Tempered Martensite at Triple Point Grain Boundary.
B.) Dislocations and Fine Precipitate Dispersion in Ferrite Grains.

Figure 19. TEM Micrograph of Non-Preheated Weldment HAZ/Base Region.
A.) Islands of Ferrite/Carbide Aggregates and Dislocations in Ferrite Grains.
B.) Precipitate and Dislocations in Ferrite Grains. Ferrite/Carbide Aggregates are Indicated.

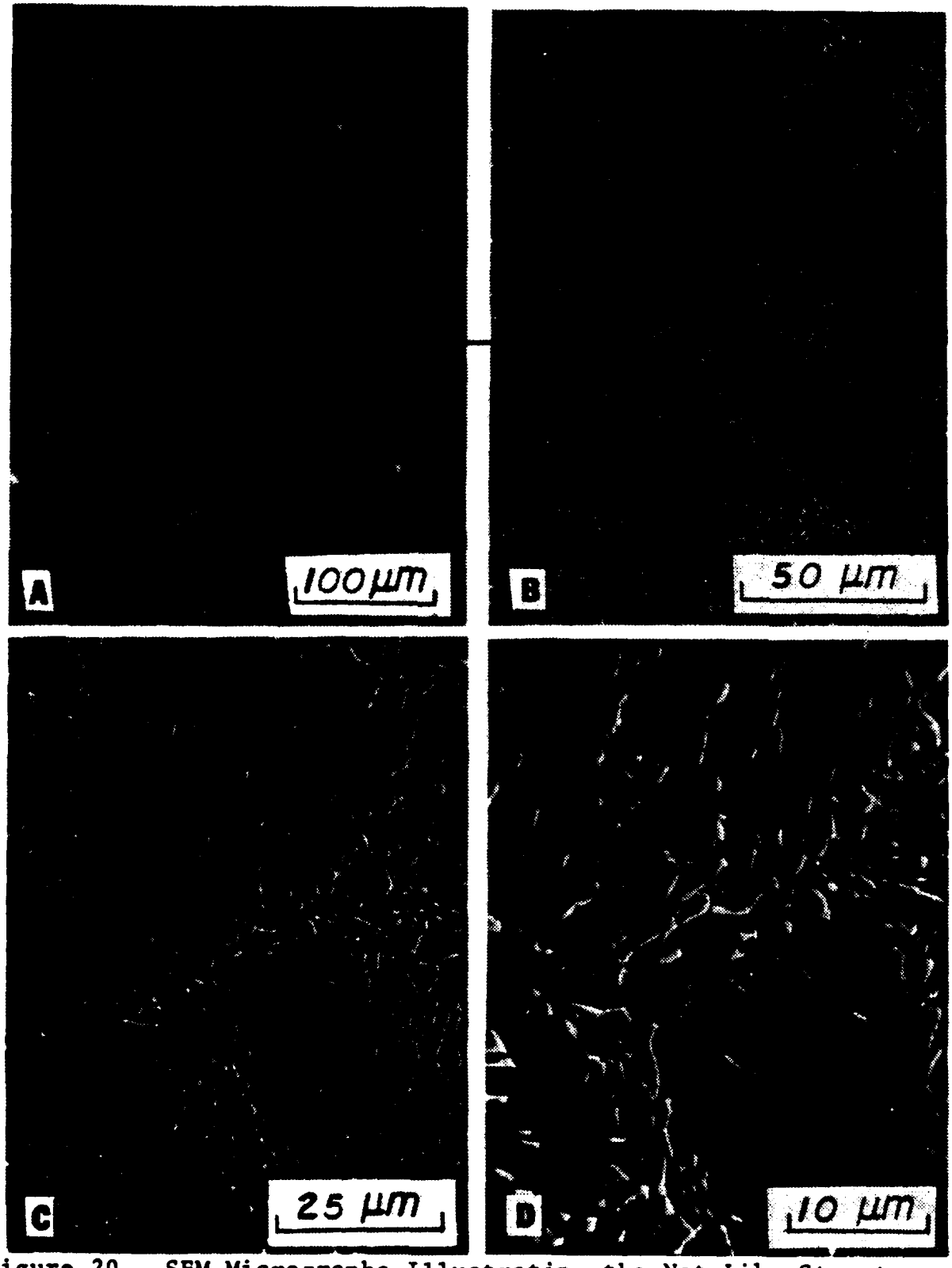

Figure 20. SEM Micrographs Illustrating the Net-Like Structure.

Figure 21. SEM Micrograph of HAZ at Fusion Line in Preheated Sample.

Figure 22. SEM Micrograph of HAZ at Fusion Line in Non-Preheated Sample.

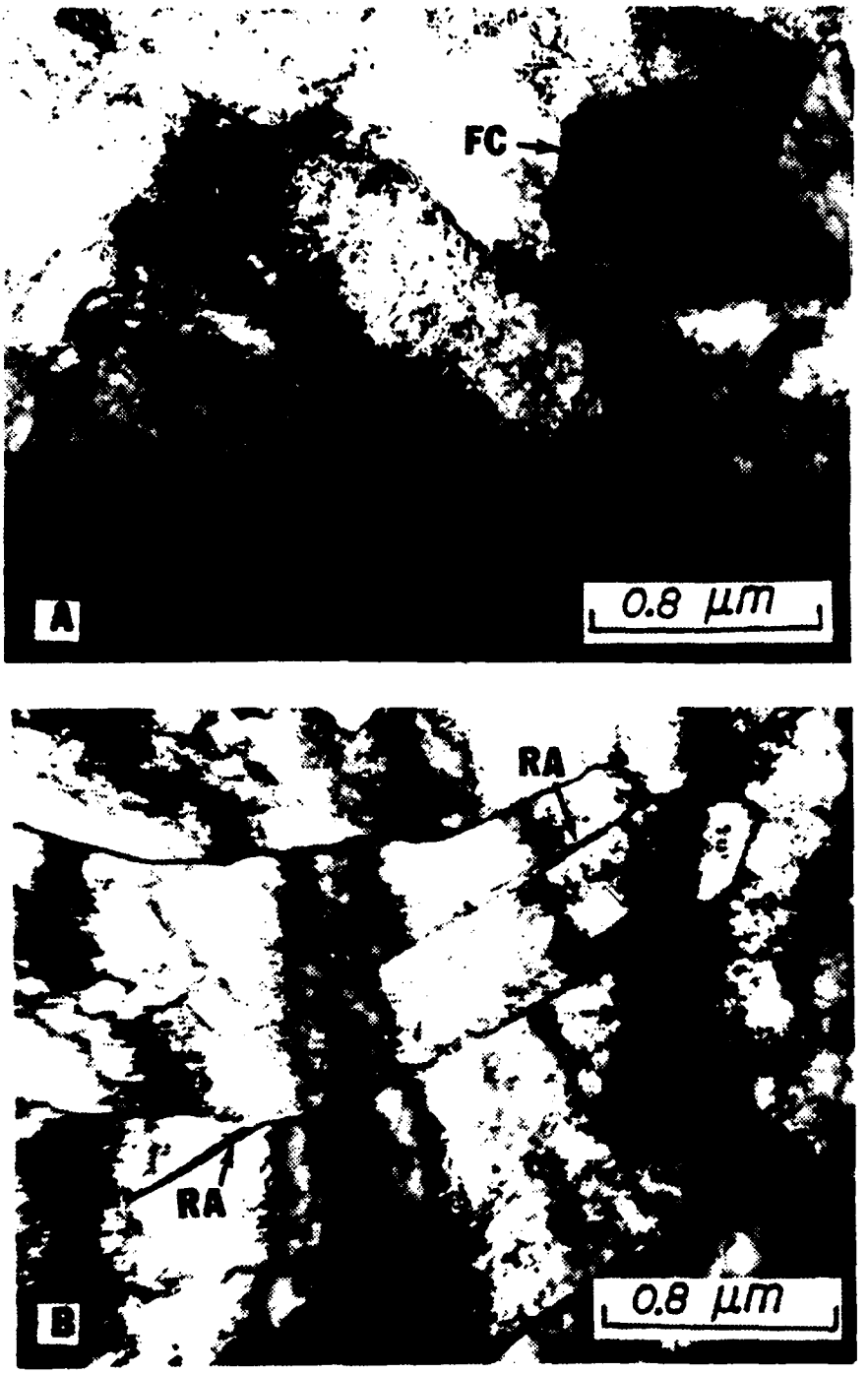

Figure 23. TEM Micrograph of Preheated Sample HAZ Region at Fusion Line.
A.) Islands of Tempered Martensite and Carbide Aggregates (FC).
B.) Acicular Ferrite Laths and Retained Austenite at the Lath Interfaces.

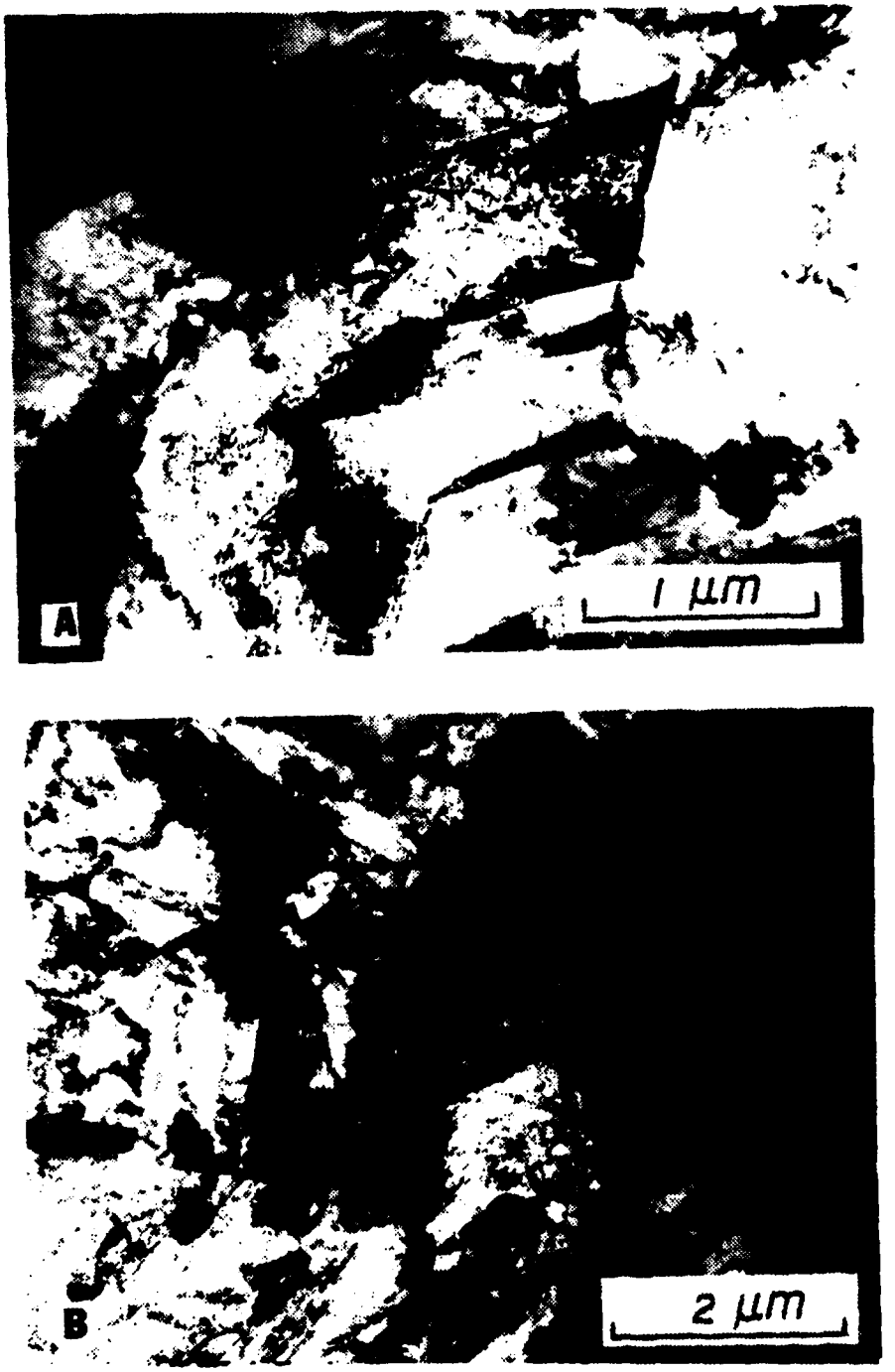

Figure 24. TEM Micrograph of Non-Preheated Sample HAZ at Fusion Line.
A.) Islands of Carbide Aggregates and Retained Austenite at Lath Interface.
B.) Islands of Carbide Aggregates.

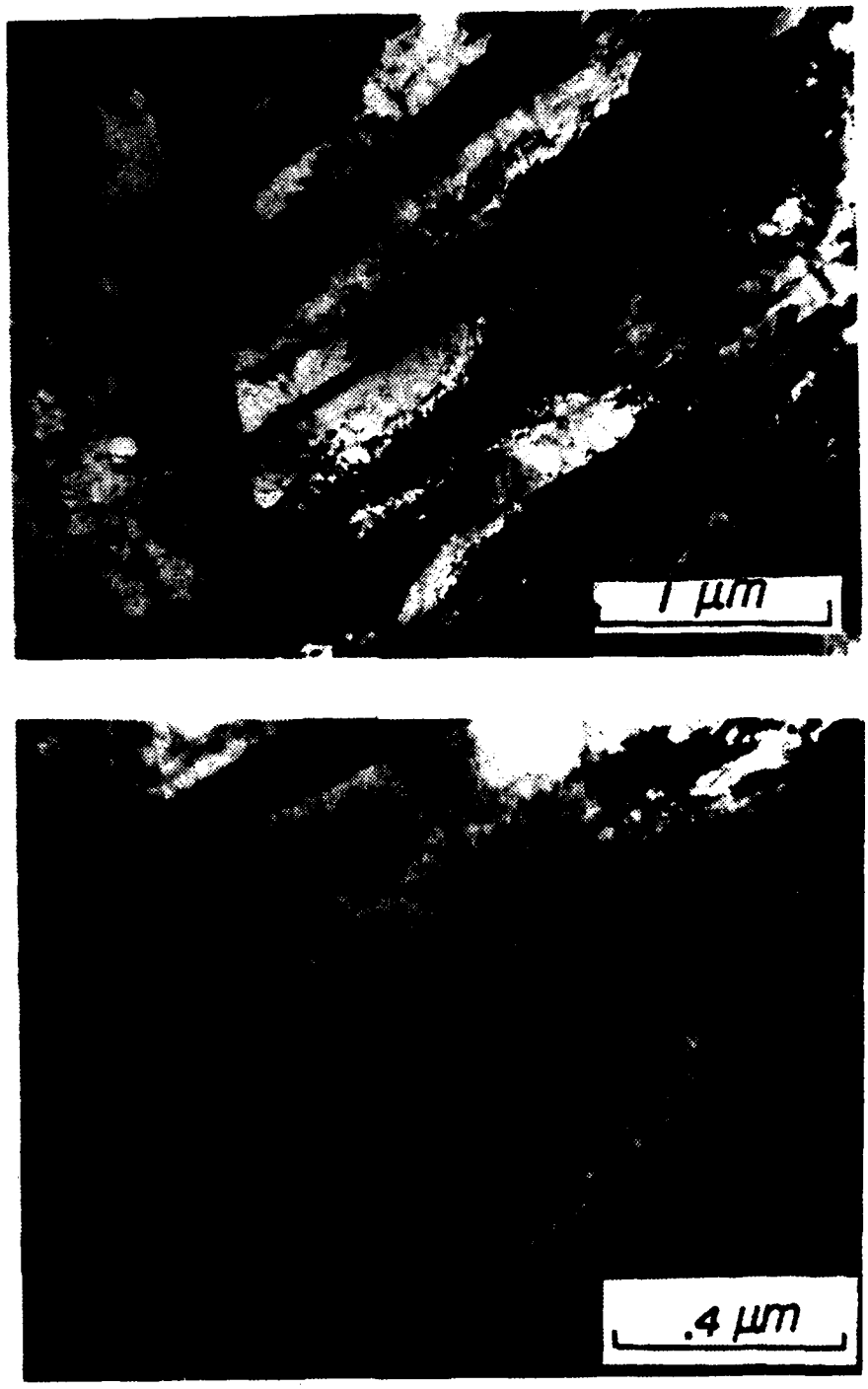

Figure 25. Example of Ferrite/Carbide Aggregates (FC) Between Ferrite Laths.

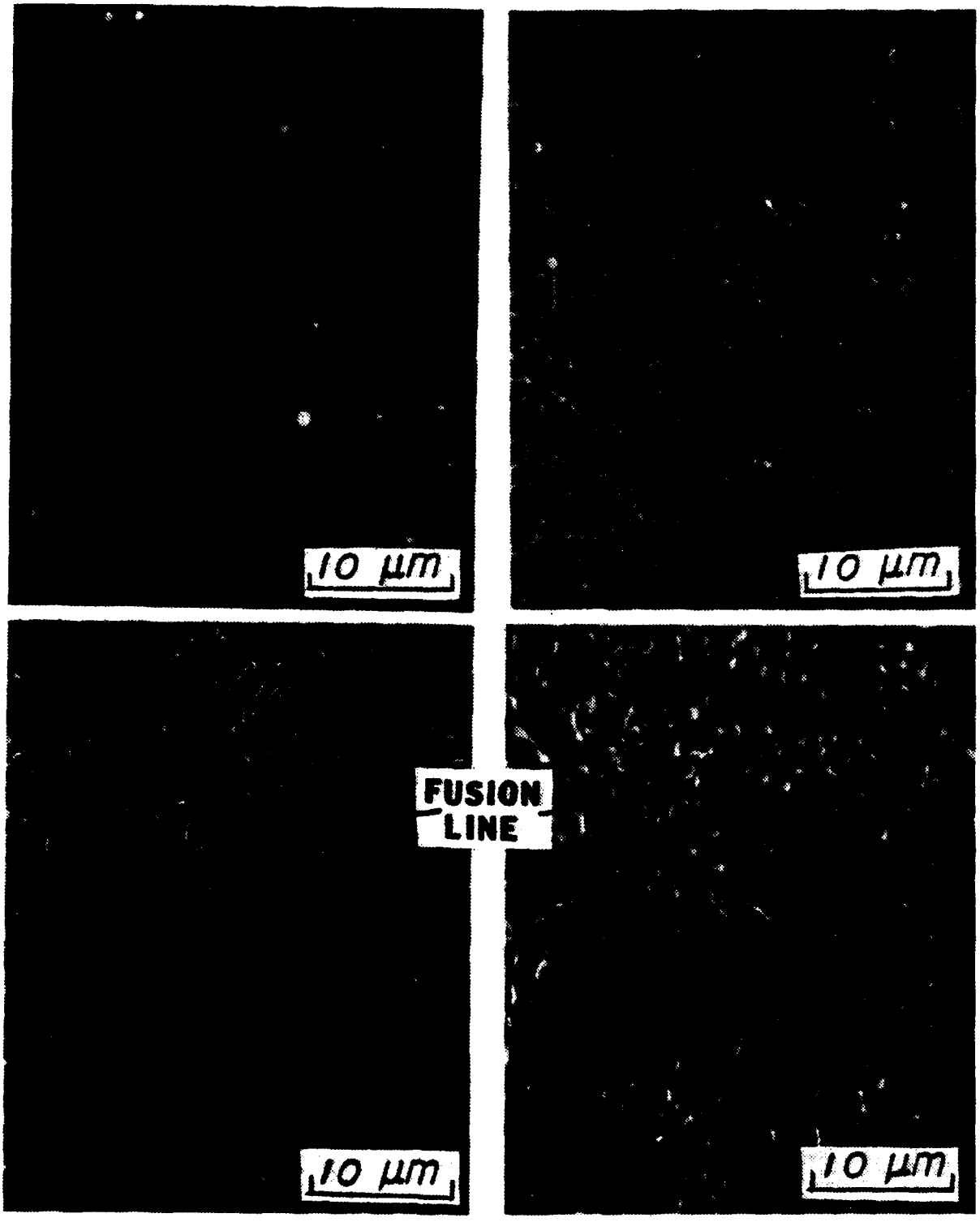

Figure 26. SEM Micrographs of Fusion Line, Melted Region, Above Fusion Line, has a Finer Grain Structure than the Adjacent HAZ Region. Upper Micrographs Reveal Numerous Inclusions.

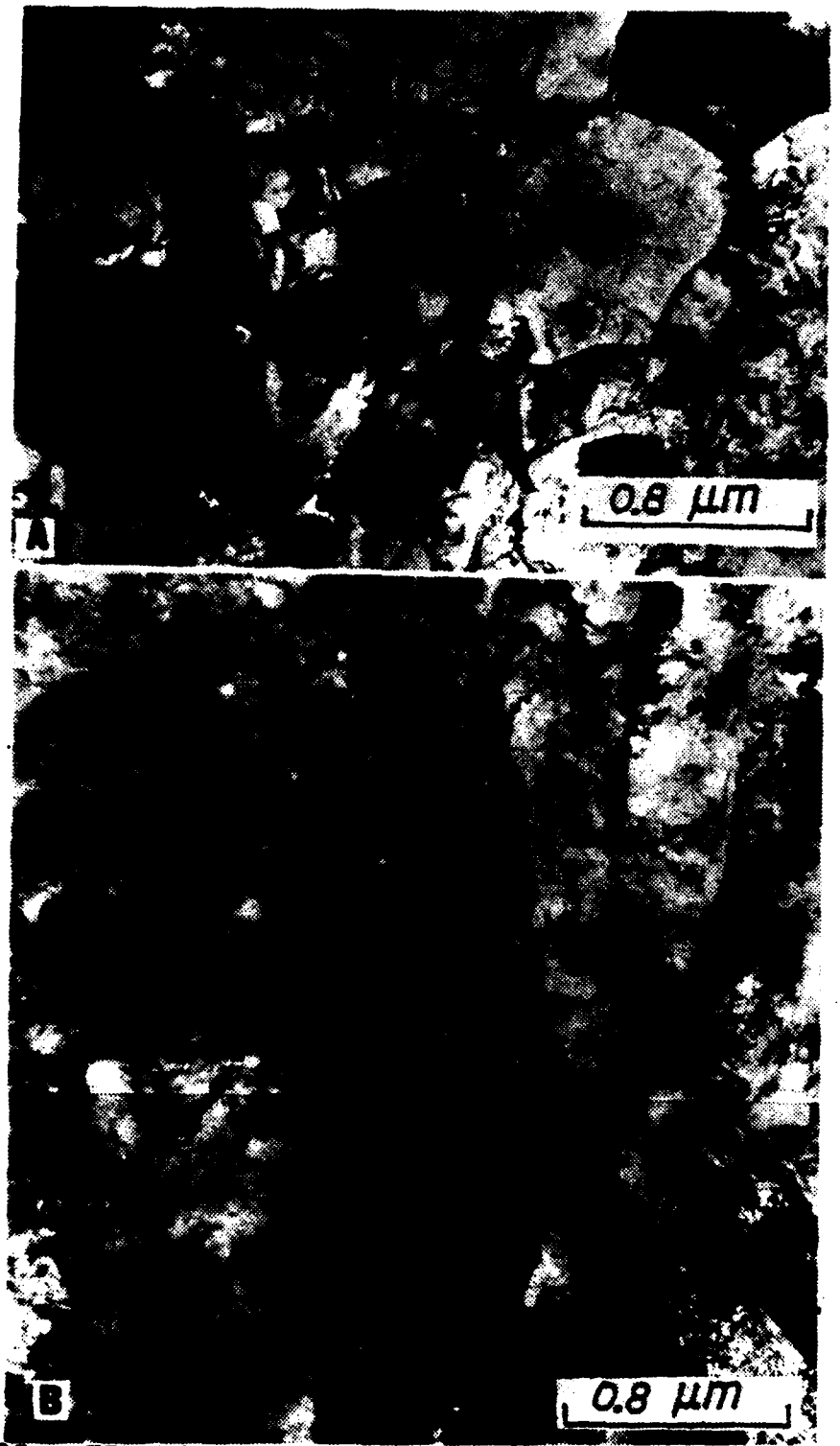

Figure 27. TEM Micrograph of Preheated Sample Mixed Region.
A.) Subgrains of Ferrite with Patch of Martensite Internally Twinned.
B.) Auto-Tempered Martensite.

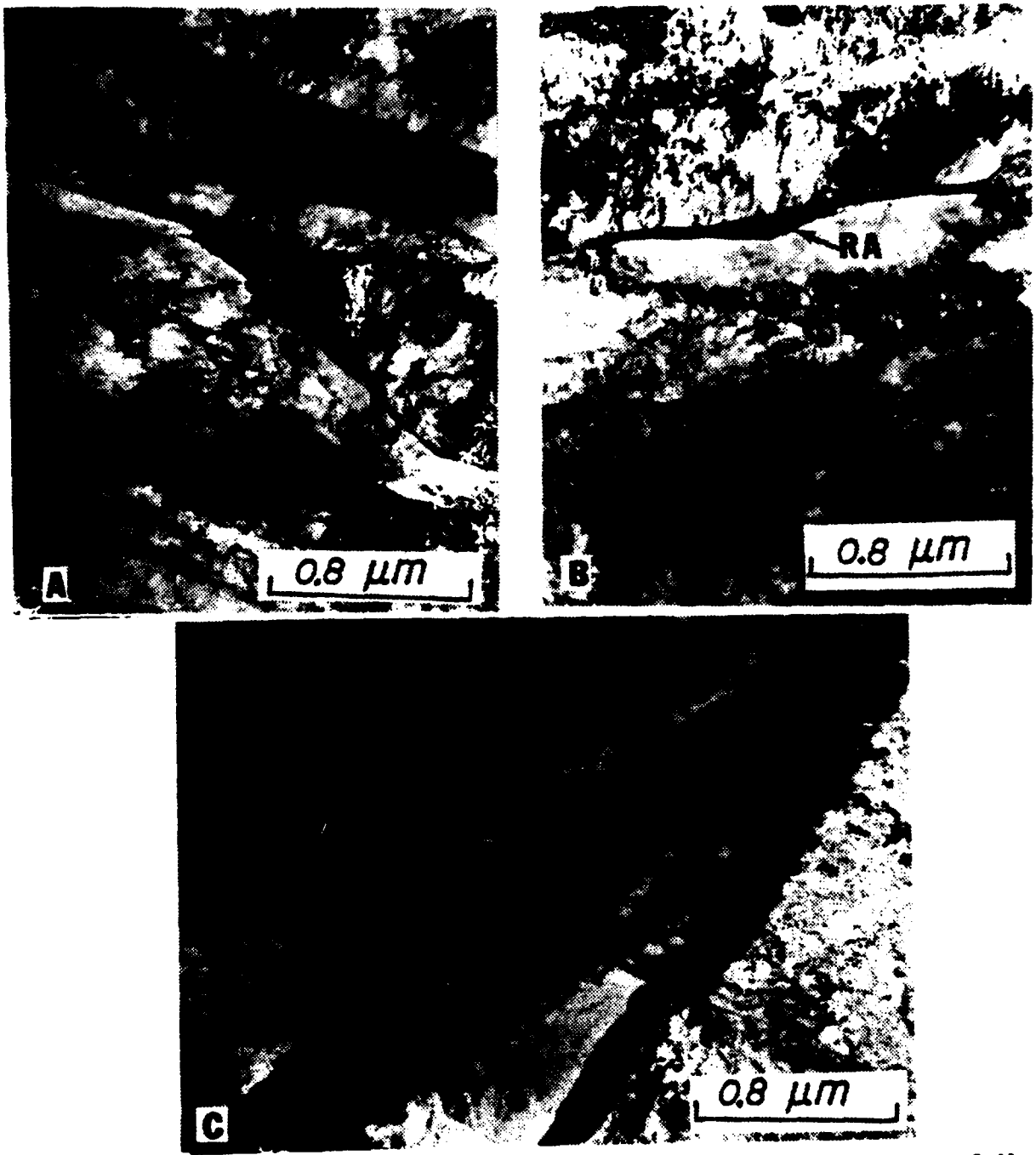

Figure 28. Typical TEM Microstructure in Mixed Region of Non-Preheated Sample.
A.) Low Carbon Tempered Martensite and Ferrite Laths.
B.) Low Carbon Tempered Martensite and a Small Path of Retained Austenite at Lath Interface of Second Lath from Right. Small Spheres are Inclusions.
C.) Enlarged View of Tempered Martensite.

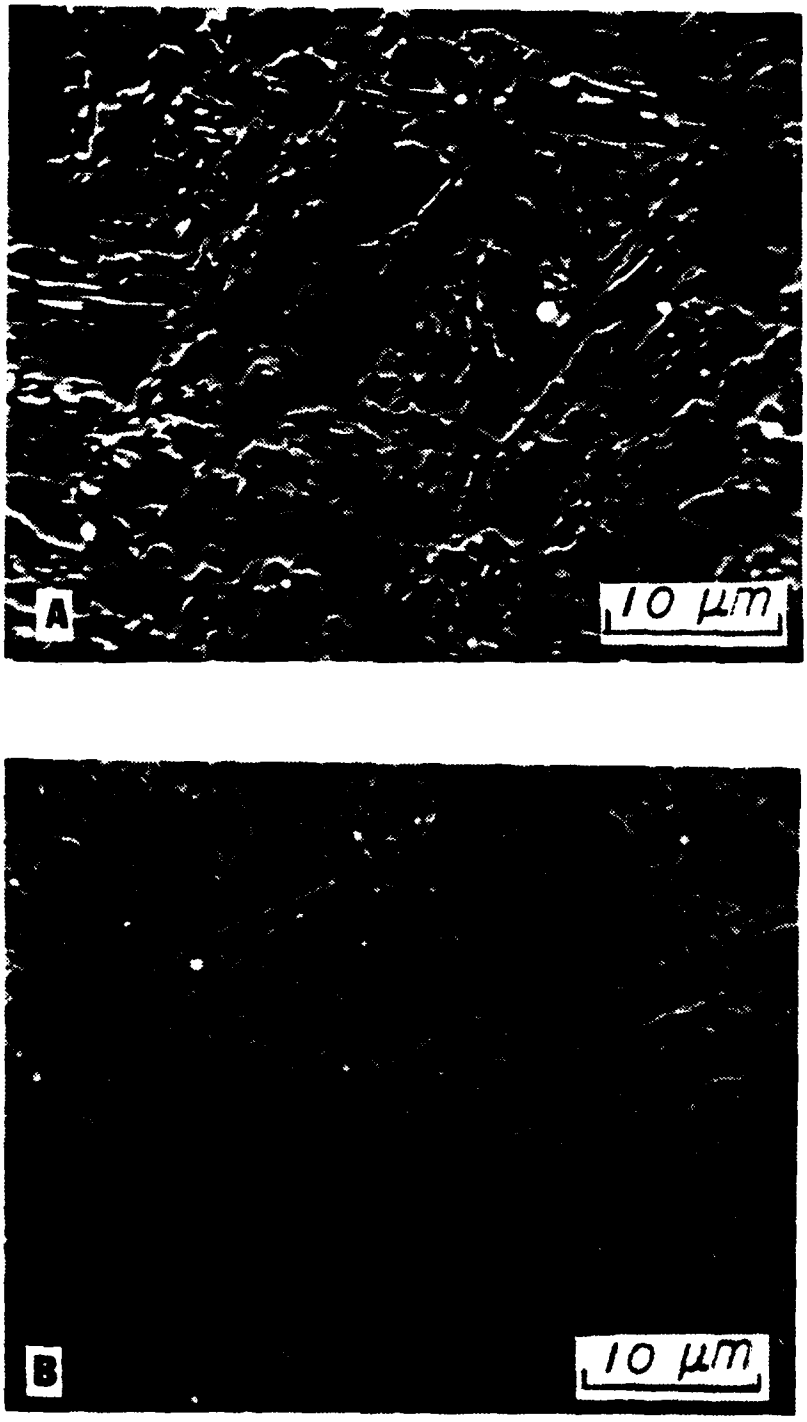

Figure 29. SEM Micrographs of Fine Grained Lath-Like Microstructure of Weld Metal.
A.) Preheated Sample.
B.) Non-Preheated Sample.

Figure 30. TEM Microstructure of Preheat Sample Weld Metal.
A.) Retained Austenite at Lath Interfaces.
B.) Islands of Tempered Martensite and Carbides on Grain Boundaries. Spheres are Inclusions.

Figure 31. TEM Micrograph of Non-Preheat Sample Weld Metal.
A.) Ferrite Laths with Patches of Retained Austenite at Lath Interfaces.
B.) Tempered Martensite and Ferrite.

LIST OF REFERENCES

1. May, I., and Krishnadev, M. R., "The Economic Exploitation of High-Strength, Low Alloy Steels: Some Recent Developments," Paper presented at Interamerican Conference on Materials Technology, pp. 445-449, August 14-17, 1972.

2. Jesseman, R. J. and Murphy, G. J., "Precipitation Hardening Alloy Steel Provides Strength and Low Temperature Toughness Under Severe Service Conditions," Industrial Heating, pp. 27-31, September 1979.

3. Meyer, L., Heisterkamp, F., and Mueschenborn, W., "Columbium, Titanium, and Vanadium in Normalized, Thermo-Mechanically Treated and Cold Rolled Steels," Proceedings, Micro Alloying 75, Union Carbide, New York, pp. 153-167, 1977.

4. Haynes, A. G., "Development and Application of NICUAGE Steels," Low Carbon Structural Steels for the Eighties, Inco Europe Limited, European Research and Development Centre, Birmigham, pp. 1138-1144, 1977.

5. Brokenshire, W. H., "IN-787 INCO's New Steel, Canadian Machinery and Metalworking, Vol. 89, No. 10, pp. 48-49, October 1978.

6. Pickering, F. B., "High-Strength, Low Alloy Steels - A Decade of Progress," Proceedings, Micro Alloying 75, Union Carbide, New York, p. 23, 1977.

7. Lancaster, J. F., Metallurgy of Welding, 3rd Edition, p. 98, George Allen and Unwin Limited, London, 1980.

8. Lancaster, J. F., pp. 155-156.

9. Lancaster, J. F., pp. 183-184.

10. "Mammoth Coal Truck Welded from Specialty Steel," Welding Journal, p. 40, November 1979.

11. Jesseman, R. J. and Schmid G. C., Submerged Arc Welding a Low Carbon, Copper-Strengthened Alloy Steel, Paper presented at the 64th Annual Meeting of the American Welding Society, April 1983.

12. Redfern, G. A. and Minard, L. C., "Welding of IN-787, An Age Hardenable Steel for Pipeline Applications," Symposium on Processing and Properties of Low Carbon Steel, Proceedings, AIME, 1973.

13. Bernard, G., "A Viewpoint on the Weldability of Carbon-Manganese and Microalloyed Structural Steels," Proceedings, Micro Alloying 75, Union Carbide, New York, pp. 552-569, 1977.

14. Hart, P. H., Dolby, R. E. and Widgery, D. J., "The Weldability of Microalloyed Steels," Proceedings, Micro Alloying 75, Union Carbide, New York, pp. 540-551, 1977.

15. Lancaster, J. F.,, pp. 131-133.

16. Redfern, G. A. and Minard, L. C., op. cit.

17. Jesseman, R. J. and Schmid G. C., op. cit.

18. Koso, M., Miura, M., and Ohmari, Y., "Microstructure and Toughness of Weld Heat-Affected Zone in 785 MN/MM HSLA Steel," Metals Technology, December 1981.

19. Department of Defense Military Specification MIL-E-22200/1E, Electrodes, Welding, Mineral Covered, Iron-Power, Low-Hydrogen Medium and High-Tensile Steel, As-Welded or Stress-Relieved Weld Application, 3 October 1978, p. 5.

20. Jesseman, R. J. and Schmid G. C., op. cit.

21. Elger, W. M., Characterization of an HY-130 Steel Weldment by Transmission Electron Microscopy, Master's Thesis, Naval Postgraduate School, p. 77, December 1981.

22. Shackleton, B., "Effect of Copper in Low Alloy and Mild Steel Weld Metals," British Welding Journal, November 1967.

23. Koso, M., Miura, M., and Ohmari, Y., op. cit.

24. Bernard, G., op. cit.

25. Jesseman, R. J. and Schmid, G. C., op. cit.

INITIAL DISTRIBUTION LIST

		No. Copies
1.	Defense Technical Information Center Cameron Station Alexandria, Virginia 22314	2
2.	Superintendent Attn: Library, Code 0142 Naval Postgraduate School Monterey, California 93943	2
3.	Department Chairman, Code 69 Department of Mechanical Engineering Naval Postgraduate School Monterey, California 93943	1
4.	Associate Professor K. D. Challenger, Code 69Ch Department of Mechanical Engineering Naval Postgraduate School Monterey, California 93943	5
5.	Mr. Rodney J. Jesseman Senior Research Metallurgist Armco Inc. Middletown, Ohio 45043	1
6.	Mr. Richard J. Wong Metallurgical Engineer David Taylor Naval Ship R & D Center Annapolis, Maryland 21401	1
7.	LT Richard F. Burna 7126 N.E. Clover Blossom Lane Bremerton, Washington 98310	5
8.	Mr. Charles Zanis David Taylor Naval Ship R & D Center Annapolis, Maryland 21401	1


FILME
3-84